

CoE: Chain-of-Explanation via Automatic Visual Concept Circuit Description and Polysemanticity Quantification

Wenlong Yu Qilong Wang* Chuang Liu Dong Li Qinghua Hu

Tianjin Key Lab of Machine Learning, College of Intelligence and Computing, Tianjin University

{yw1_95, qlwang, liuc_09, li_dong, huqinghua}@tju.edu.cn

Abstract

Explainability is a critical factor influencing the wide deployment of deep vision models (DVMs). Concept-based post-hoc explanation methods can provide both global and local insights into model decisions. However, current methods in this field face challenges in that they are inflexible to automatically construct accurate and sufficient linguistic explanations for global concepts and local circuits. Particularly, the intrinsic polysemanticity in semantic Visual Concepts (VCs) impedes the interpretability of concepts and DVMs, which is underestimated severely. In this paper, we propose a **Chain-of-Explanation (CoE)** approach to address these issues. Specifically, CoE automates the decoding and description of VCs to construct global concept explanation datasets. Further, to alleviate the effect of polysemanticity on model explainability, we design a concept polysemanticity disentanglement and filtering mechanism to distinguish the most contextually relevant concept atoms. Besides, a Concept Polysemanticity Entropy (CPE), as a measure of model interpretability, is formulated to quantify the degree of concept uncertainty. The modeling of deterministic concepts is upgraded to uncertain concept atom distributions. Finally, CoE automatically enables linguistic local explanations of the decision-making process of DVMs by tracing the concept circuit. GPT-4o and human-based experiments demonstrate the effectiveness of CPE and the superiority of CoE, achieving an average absolute improvement of 36% in terms of explainability scores.

1. Introduction

Deep learning-based vision models have demonstrated outstanding performance in various visual tasks, owing to the powerful learning and representation capabilities of deep neural networks (DNNs) [38, 66]. However, the extreme complexity of DNNs, while enhancing their performance, also limits their explainability [53]. Humans are often un-

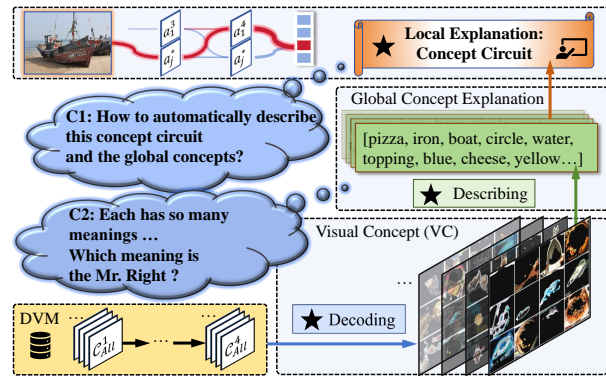


Figure 1. Illustration of the integrated process of concept-based post-hoc XAI methods [46], along with two challenges they face.

aware of the reasons behind the model’s conclusions. This lack of explainability significantly hinders the wide application of deep vision models (DVMs) in critical fields such as autonomous driving and medical diagnosis [9, 37].

Post-hoc eXplainable Artificial Intelligence (XAI) can enhance the transparency of DVMs without causing degradations in performance [43, 55]. Research in this field can roughly be divided into local and global XAI methods [8]. The former explains either specific stages or the entire decision path with respect to a specific sample, identifying key activated regions or significant semantic concepts [5, 58, 60]. The latter deciphers the overall behavior of the DVM in a dataset by concept discovery or visualization techniques [29, 36, 68]. Among them, concept-based methods can explain DVMs from both global and local (glocal) perspectives [3, 6], assuming that each channel or neuron in a certain layer is responsible for recognizing essential semantic concepts. As shown in Fig. 1, they primarily perform one or two of the three operations: decoding Visual Concepts (VCs) of DVMs, manually constructing global concept explanation datasets, and providing local concept circuit explanations for individual samples [18, 21, 35].

Despite the significant progress made in concept-based explanation research, certain challenges remain, as illustrated in Fig. 1. First, the VCs are decoded by manually

*Corresponding author. Published in CVPR 2025.

identifying and annotating the commonalities of a set of extracted image patches [3, 35]. These manual methods intuitively become ineffective when faced with new scenarios, new models, and new XAI methods, due to high labor costs, low efficiency, and the limited cognitive scope of individual annotators. Second, most methods make a naive assumption: each concept is monosemantic and user-friendly [42]. However, in practice, VCs encapsulate polysemantic information [30] (*e.g.*, an average of 13 concept atoms are coupled per channel in a ResNet152 model), presenting challenges for the model explanation. Particularly, polysemanticity can serve as a metric for evaluating a model’s interpretability. A higher level of polysemanticity signifies a broader conceptual space, increasing the risks of selecting incorrect semantics and generating deviated explanations. Arbitrary concept selection or presenting them solely as images without descriptions yields suboptimal explanations [55]. Both visualizations and linguistic explanations become challenging for humans to comprehend, as it is unclear which semantic is actually represented or holds prominence [21]. Although polysemanticity is crucial to XAI, its systematic quantification and resolution remain unaddressed. All of these challenges collectively exacerbate the difficulty of concept-based explanations for DVMs.

To alleviate this dilemma, we propose a Chain-of-Explanation (CoE) approach via automatic concept decoding, disentanglement, filtering, description, and polysemanticity quantification. Specifically, CoE first proposes an Automatic Concept decoding and Description (ACD) method to construct global concept explanation datasets. It decodes every VC of key layers through arbitrary advanced XAI methods. A Large Vision Language Model (LVLM) is utilized to describe the commonalities of the extracted image patches since the linguistic explanation is more comprehensible than images [55]. As for the polysemantic concepts, we formulate a Concept Polysemanticity Disentanglement and Filtering (CPDF) mechanism to disentangle them into a set of orthogonal concept atoms, along with a Concept Polysemanticity Entropy (CPE) to quantify their degree of polysemanticity. In this paper, 13 distinct semantic directions are prompted, including low-level and high-level semantics, which is much more than previous work (*e.g.*, 5 in [74]). Within the CPDF, a semantic entailment model is applied to mitigate the impact of redundant semantics. After these operations, the modeling of deterministic concepts is upgraded to uncertain concept atom distributions. When elucidating the local decision-making process, a concept circuit method is utilized to form the basis of an explanation chain, with each node representing a hierarchical set of essential concepts. Relevant atoms and their interconnections are contextually filtered and aligned within the chain. Finally, we consolidate all conceptual information along the explanation chain to generate linguistic explanations similar

to a Chain-of-Thought (CoT) pipeline [27, 67], leveraging a Large Language Model (LLM), as shown in Fig. 2. Qualitative and quantitative experiments validate the effectiveness and the superiority of the CoE approach. The contributions of this paper are summarized as follows.

- We propose a novel CoE approach to automatically and systematically provide concept-based global explanations, along with managing the problem of polysemanticity, in a more interpretable natural language format.
- A CPDF mechanism is formulated to handle the hard-to-interpret polysemantic concepts. To our knowledge, CPDF is a pioneer tailored to comprehensively disentangle and quantify polysemanticity. It disentangles them into a set of succinct concept atoms, followed by a filtering function to contextually find the suitable atom as the explanation node. A CPE score is defined to quantify the polysemanticity of concepts, which can be utilized as a metric of the interpretability of concepts or models.
- Both GPT-4o and human-based experiments validate the superiority of the CoE in automatically constructing global and local explanations and the effectiveness of CPE in quantifying concept polysemanticity.

2. Related Work

Research on XAI can be broadly categorized into ad-hoc model interpretability and post-hoc explanation studies [55, 70]. The former actively refine DVMs to improve interpretability while also necessitating consideration of a trade-off between performance and interpretability [10, 40, 47, 54, 71]. The latter explains DVMs passively without performance decline [7, 13, 29, 58, 60]. Among these post-hoc efforts, concept-based explanations can provide global insights into DVMs [46]. Literature [74] annotated every pixel in special datasets with only 5 kinds of concepts. The explanation is derived by analyzing the activation regions of each neuron. MILAN [35] decoded VCs by calculating the maximum mutual information between channels and regions, followed by manually summarizing commonalities into 3 sentences. However, defining concepts solely through activations is insufficient. CRP decoded VCs through the relevance value derived from the deep Taylor decomposition [44], showing more accurate results than the activation-based methods [3]. The commonalities of the VCs were also identified manually, and one of these commonalities was selected randomly. However, these methods encounter significant challenges, as discussed in Sec. 1. In contrast, this paper proposes an automated concept decoding and description method based on LVLM, which offers greater flexibility in providing linguistic explanations. The most suitable concepts for interpretation are contextually selected, showing superior results.

Circuits, as sub-graphs, are proposed to explain the key decision route of a model [5, 17, 22, 25, 63]. They identify

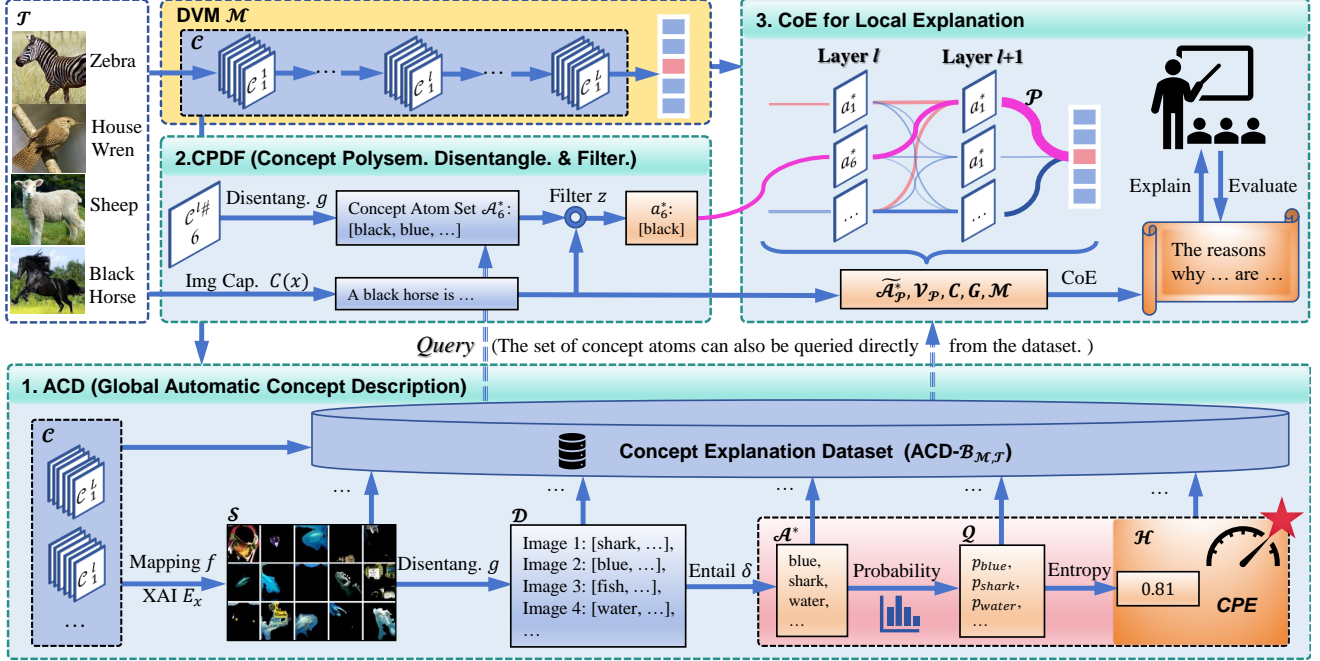


Figure 2. Outline of the Chain-of-Explanation. It consists of three steps (i.e., ACD, CPDF, and local explanation). Each part utilizes a set of channels \mathcal{C} from \mathcal{M} . In the concept circuit, \mathcal{P} , lines of different depths and colors represent the magnitude of the relevance.

the highest-activated concepts and then explain the model’s decision by linking all concepts across the circuit. However, its interpretability for DVMs is limited due to the lack of a cohesive, language-based explanatory output. Additionally, the polysemanticity of VCs significantly hinders the accurate explanation [23, 42], and research in this area remains limited. Some methods attempted to indirectly mitigate its impact by predefining principal vectors or subspaces [25, 36, 49]. The lack of flexible and accurate concept-level explanations also restricts their adaptability. Literature [42] analyzed the polysemanticity from an information compression perspective. Pure [21] alleviated the polysemanticity by clustering and decoupling the circuit route. These methods, however, lack the ability to simultaneously and comprehensively quantify, disentangle, and describe polysemantic VCs. Their applicability is limited—challenges that this paper seeks to address, as discussed in Sec. 3.

3. Chain-of-Explanation Approach

In this paper, a CoE approach is proposed to automatically explain DVMs from both global and local perspectives. It breaks down the complex reasoning path into a chain of concept nodes, within which polysemanticity is effectively managed. As shown in Fig. 2, CoE is composed of three steps. **Step 1:** ACD is proposed to automatically construct global concept descriptive explanation datasets of a given DVM. **Step 2:** With the assistance of an LVLM, a CPDF mechanism is designed to disentangle each original VC into

a set of concept atoms and extract the most suitable atom according to the context, making CoE more comprehensible and flexible. Besides, a CPE score is formulated accordingly to quantify the degree of polysemanticity of concepts. **Step 3:** A local explanation chain in a manner akin to a CoT for the decision-making progress of the DVM is established based on the dataset, CPDF, concept circuit, and LLMs.

3.1. Automatic Concept Decoding and Description

ACD method is first formulated to automatically and effectively construct databases of global concept descriptions. Specifically, given an image dataset \mathcal{T} and a DVM \mathcal{M} requiring evaluation and explanation, we establish an injective function f between channel set \mathcal{C} and visual semantic concept set \mathcal{S} by an XAI method E_x , $f: \mathcal{C} \mapsto \mathcal{S}$. Without loss of generality, for j th channel c_j^l in layer l , E_x extracts a set of image patches within \mathcal{T} that most activate this channel, named VC $s_j^l = \{I_n\}_N$, where N is the number of image patches. Each I_n highlights certain regions of the original image, representing the focused concept, as exemplified in the bottom left part of Fig. 2.

A describing function r is then defined to decipher $\{I_n\}_N$ into a set of language descriptions:

$$\mathcal{D} = r(\{I_n\}_N) = \{d_m\}_M, \quad (1)$$

where M is the number of language descriptions for the current channel. Traditionally, r is implemented by manually and subjectively identifying commonalities within $\{I_n\}_N$ [74], while ACD utilizes a powerful LVLM as the describer

with well-engineered prompts. After constructing \mathcal{S} , \mathcal{D} and the mapping function f , a concept description dataset $\mathcal{B}_{\mathcal{M},\mathcal{T}} = \{\mathcal{C}, \mathcal{S}, \mathcal{D}, f\}$ is automatically constructed, providing global linguistic explanations for all VCs of \mathcal{M} .

3.2. Managing Polysemantic Concept

Vcs of each node within a DVM exhibit polysemanticity, introducing certain deviations in the explanation framework, as shown in Fig. 2. Higher polysemanticity indicates that the current VC aggregates more semantics, making the intended representation more ambiguous. Such semantic uncertainty impedes human comprehension of the concept, particularly within the CoE, where various concepts must be understood collectively. Quantifying and solving this dilemma is difficult and has been underestimated by previous studies. Under this circumstance, we propose a CPDF mechanism along with a CPE score to mitigate and quantify its detriments to the CoE simultaneously.

3.2.1 Polysemantic Concept Decoupling and Filtering

Considering that a polysemous word can be understood as an aggregation of various distinct meanings, we define a function g to disentangle the ambiguous VC into a set of easily understandable linguistic concept atoms:

$$\mathcal{A} = \{a^1, \dots, a^i, \dots, a^Q\} = g(s), \quad (2)$$

where Q is the number of the concept atoms. We posit that each atom represents a view of the current VC s , which will be activated upon the appearance of the corresponding semantic in the input. Furthermore, given that concept atoms should accurately represent the commonalities in $\{I_n\}_N$ and recognizing that this naive disentanglement function (Eq. 2) does not provide a foundation for quantifying polysemanticity, we refine the function g to disentangle each image patch I_n into a set of atoms:

$$\begin{aligned} \mathcal{A}_n &= \{a_n^1, \dots, a_n^i, \dots, a_n^Q\} = g(I_n, s), \\ \mathcal{D} &= \{\mathcal{A}_n\}_N. \end{aligned} \quad (3)$$

We instantiate g by a powerful LVLm (e.g., GPT-4o [50]), considering that this is quite an open and complex problem. g prioritizes disentangling and describing commonalities within the VC while analyzing each individual image. Various commonalities among any certain number of image patches should be summarized and described by precise terminologies. These common semantics within an open scenario are as diverse as they are abundant, unfolding in countless forms and nuances. Besides, it should generate specific atoms when any commonalities identified above do not appear in the current I_n . Therefore, the art of prompt engineering `prompt-com` becomes paramount. It should provide rules for recognizing commonalities, possible conceptual directions, and output format control. In

this paper, we prompt 13 high-level and low-level semantical directions that cover the normal concepts encountered in daily life, including object category, scene, object part, color, texture, material, position, transparency, brightness, shape, size, edges, and their relationships. Additionally, the CoT techniques [27, 67] are introduced. Details of all sophisticated prompts are shown in Sec. S2 of the Appendix.

All \mathcal{A}_n are then aggregated into a description atom set \mathcal{A} with all duplicate atoms removed:

$$\begin{aligned} \mathcal{A} &= \{\mathcal{A}_1 \cup \mathcal{A}_2 \cup \dots \cup \mathcal{A}_N\} \\ &= \{a^1, \dots, a^i, \dots, a^P\}, \end{aligned} \quad (4)$$

where P is the number of concept atoms after deleting the repeating atoms. Each element in \mathcal{A} represents a disentangled monosemantic concept and can be utilized as a node of the CoE. However, some atoms are semantically equivalent even if they have variant descriptions [24]. In order to remove semantically redundant atoms, we introduce an entailment function δ to detect the relations between atoms:

$$\{1, 0, -1\} = \delta(a^{i1}, a^{i2}), \forall a^{i1}, a^{i2} \in \mathcal{A}, \quad (5)$$

where the responses 1,0,-1 represent entailment, neutral, or contradiction of the candidates, respectively. We instantiate δ by an NLI model (e.g., DeBERTa model [33]) because the atom candidates are relatively short and simple that an NLI model is good enough. Following [24], a bidirectional entailment check is applied, meaning that one of the candidates will be removed when the response is entailment or neutral. The first atom is designated as the monosemantic representative of the semantic equivalence set due to the transitivity between them. The final concept set \mathcal{A}^* only contains heterogeneous atoms that describe the current VC:

$$\mathcal{A}^* = \{a^1, \dots, a^i, \dots, a^{P^*}\}. \quad (6)$$

After disentangling the concept atoms, we define a filtering function z to select an atom a^* as the most suitable explanation of current VC with respect to the input x :

$$a_s^*(x) = z(\mathcal{A}_s^*, C(x)). \quad (7)$$

Some research ignores this step or selects the concept randomly with an implicit assumption that all concepts in \mathcal{A}^* are semantically equivalent [18, 35]. In contrast, we filter the most suitable atom a^* based on the context of the CoE. In particular, z is instantiated by an LLM. $C(x)$ is an image captioning function utilized for providing contextual information. It can be instantiated by a relatively small LVLm [11, 12] or a professional model [39, 64].

3.2.2 Quantification of Concept Polysemanticity

The polysemanticity of concepts can serve as a metric for the model’s interpretability. Lower polysemanticity of concepts indicates reduced semantic uncertainty with a more

singular form of activation, leading to greater interpretability. In this paper, we endeavor to quantify polysemanticity from three levels of granularity (i.e., conceptual channels, layers, and models) by defining a CPE score. The larger the CPE, the more pronounced the polysemanticity, which leads to decreased interpretability.

In particular, the disentanglement function g in Eq. 3 enables us to count the frequency of each atom in \mathcal{A}^* . Given two fixed numbers Q and N , we calculate the probability of the i_{th} atom within j_{th} concept:

$$p_i = \frac{Num_i}{Q \times N + Pad}. \quad (8)$$

Then, the CPE of j_{th} concept can be formulated as

$$H_j^* = \frac{-\sum_{i=1}^{P^*+Pad} p_i \log p_i}{\log(P^* + Pad)}. \quad (9)$$

The denominator normalizes the entropy value to a range between 0 and 1, considering that the size of P^* varies for different VCs. Besides, the quantity of \mathcal{A}^* is set to be at least equal to N due to some \mathcal{D}_s having a small number of semantical equivalent atoms with equal probabilities. If there are insufficient unique atoms, we supplement the corresponding number of atoms, with each supplementary atom set to a number of 1. The atomic objects are expanded, and the denominator is increased by the number of supplemented atoms (a total amount of Pad). Please refer to Sec. S3.1 of the Appendix for details. In addition, two averaged CPEs are formulated to enable comparisons of polysemanticity between specific layers or models:

$$H_i^* = \frac{1}{d_i} \sum_{d_i} H_j^*, \quad (10)$$

$$H_{\mathcal{M}}^* = \frac{1}{L} \sum^L H_i^*, \quad (11)$$

where d_i is the dimension of the channel and L is the number of layers. Finally, to accommodate the diverse needs of researchers within the community, the automatically constructed concept explanation dataset is extended as $\text{ACD-}\mathcal{B}_{\mathcal{M},\mathcal{T}} = \{\mathcal{C}, \mathcal{S}, \mathcal{D}, \mathcal{A}^*, \mathcal{Q}, \mathcal{H}, f\}$, where \mathcal{Q} represents the probability set of each atom and \mathcal{H} is the set of CPE.

3.3. Construction of Explanation Chain

Concept circuits in DVMs can identify the most activated units in each layer for a specific input [5]. When aggregating these units across all key layers in a bottom-up manner, a corresponding maximum activation path \mathcal{P} is generated, establishing the foundation for the explanation chain. Each node in this path serves as the explanation for the model’s decision at that layer. Traditional concept circuit methods for DVMs identify the activation path without providing thorough overarching natural language-based explanations. Inspired by the CoT explanation technique in LLMs

[16], CoE proposes a local explanation chain to interpret the decision-making process of DVMs in the form of natural language descriptions based on $\text{ACD-}\mathcal{B}_{\mathcal{M},\mathcal{T}}$, CPDF, concept circuit method, and LLM, as shown in Fig. 2.

Specifically, some user-predefined layers requiring explanations or key layers facilitating CoE (e.g., output layers of 4 stages of a DVM) are listed in a bottom-up manner. Given an image x and layer l , an advanced XAI method E_x computes the maximization normalized activation or relevance values for all concepts. Each value represents the importance of the current concept to the prediction $\mathcal{M}(x)$. CoE acknowledges top k^l relevant concepts $\mathcal{C}^l(x) = \{c_1^l, \dots, c_{k^l}^l\}$ and their values $\mathcal{V}^l(x) = \{v_1^l, \dots, v_{k^l}^l\}$, determined by the α quantile of relevance values across all concepts (i.e., $k^l = |\{v_j^l | v_j^l > \alpha \max(v^l), \forall j \in d^l\}|$, where $|X|$ computes the number of elements). After that, the descriptive concept atoms of the current layer $\tilde{\mathcal{A}}_{k^l}^{*l}(x) = \{a_1^{*l}, \dots, a_{k^l}^{*l}\}$ are constructed based on $\text{ACD-}\mathcal{B}_{\mathcal{M},\mathcal{T}}$ and the filter Eq. 7, serving as a node of the explanation chain.

The final CoE for the local decision-making explanation, abstracting and synthesizing all top activated concept atoms along the chain, is formulated as

$$CoE_{\mathcal{M}}(x) = e(\tilde{\mathcal{A}}_{\mathcal{P}}^*(x), \mathcal{V}_{\mathcal{P}}(x), C(x), G(x), \mathcal{M}(x)), \quad (12)$$

where e formulates a synthesizing and describing function with inputs obtained from the above sections, and $G(x)$ is the label of x . We instantiate $CoE_{\mathcal{M}}(x)$ through a powerful LLM (e.g., GPT-4 [1]), with prompt `prompt-coe` well-designed by combining CoT and few-shot prompting [56].

Additionally, these local explanations are evaluated by a powerful LVLM and human judges based on three explainability metrics, each utilizing a three-tier scoring system.

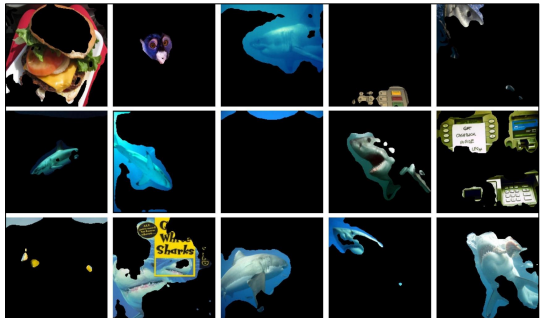
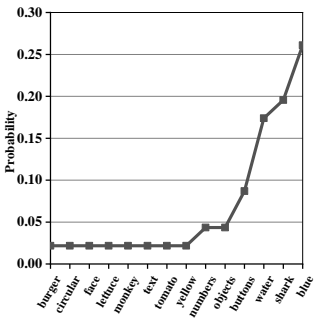
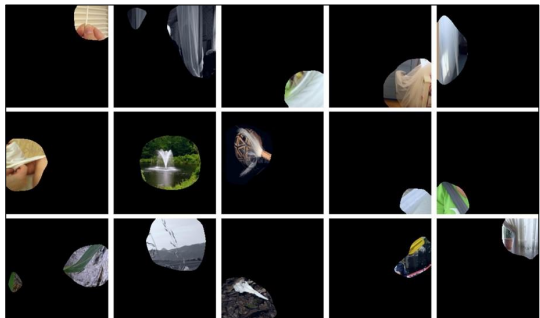
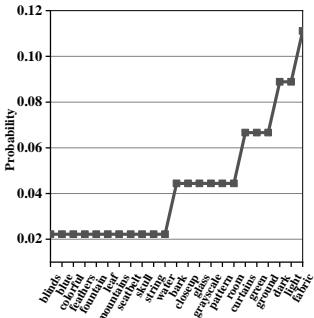
4. Experiments

We evaluate the proposed CoE approach on two types of DVMs (i.e., ResNet [32] and CLIP [52]). The relevance-based XAI method CRP is adopted as the primary approach for E_x in this paper, owing to its demonstrated superiority in terms of fidelity and reliability [3]. Please refer to the Appendix for more details on the implementation and results. Codes are available at <https://github.com/YuWLong666/CoE>.

4.1. Concept Explanation Dataset Construction

In the CoE, we first automatically construct global concept description databases $\text{ACD-}\mathcal{B}_{\mathcal{M},\mathcal{T}}$ for various DVMs. Taking a ResNet152 model as an example, 4 output layers of 4 stages (with 256, 512, 1024, and 2048 channels \mathcal{C} , respectively) are selected as the key layer set. CRP is applied as E_x to extract the VC set \mathcal{S} . Following [3], each VC is represented by 15 (i.e., N) image patches. The mapping function

Table 1. Examples of VCs and their disentangled concept atoms, along with their concept probability distributions and CPE scores. The first row shows concept 75 of Layer 4 extracted by CRP. The second row shows concept 697 of Layer 4 extracted by MILAN.

Visual Concept and Disentangled Concept Atoms		Concept Distribution	CPE
	<p>Image 1: [burger, lettuce, tomato], Image 2: [blue, monkey, face], Image 3: [shark, blue, water], Image 4: [keypad, buttons, numbers], Image 5: [shark, blue, water], Image 6: [shark, blue, water], Image 7: [shark, blue, water], Image 8: [blue, circular, shape], Image 9: [shark, blue, water], Image 10: [keypad, buttons, numbers], Image 11: [blue, yellow, objects], Image 12: [shark, blue, text], Image 13: [shark, blue, water], Image 14: [shark, blue, water], Image 15: [shark, blue, water]</p>		0.81
	<p>Image 1: [hand, blinds, string], Image 2: [curtains, room, grayscale], Image 3: [fabric, green, closeup], Image 4: [curtains, room, light], Image 5: [reflection, glass, light], Image 6: [hand, fabric, texture], Image 7: [water, fountain, greenery], Image 8: [feathers, pattern, dark], Image 9: [fabric, blue, closeup], Image 10: [fabric, green, seatbelt], Image 11: [leaf, bark, texture], Image 12: [nature, mountain, grayscale], Image 13: [skull, ground, dark], Image 14: [fabric, colorful, pattern], Image 15: [curtains, window, light]</p>		0.95

f from channels to VCs is built. We then employ a GPT-4o-2024-08-06 model as the function g to generate the description set \mathcal{D} (i.e., Eq. 3). The disentangled and clustered atom set \mathcal{A}^* (processed by a DeBERTa model), the probability set \mathcal{Q} , and the CPE set \mathcal{H} are computed and gathered accordingly. Overall, $\text{ACD-}\mathcal{B}_{\mathcal{M},\mathcal{T}}$ containing 3,840 entries is constructed, with each entry comprising a channel, a CPE score, and 15 VC representations—each consisting of 3 concept atoms (i.e., Q)—and multiple orthogonal linguistic atoms, along with their associated probabilities.

4.2. Disentanglement of Polysemantic Concept

CPDF automatically disentangles and describes the polysemantic VCs into a set of linguistic concept atoms, \mathcal{D} . As exemplified by Table 1, two randomly selected VCs are extracted by two advanced XAI methods (CRP and MILAN). They are disentangled and described into atoms, exhibiting different degrees of polysemanticity. We observe that the commonalities within the VCs are almost entirely identified, and most of the atoms describe the commonalities of subsets of image patches. In the first row (CPE=0.81), g successfully identifies all visually discernible commonalities, such as shark and water. The atoms exhibit high consistency, and fewer but more frequently occurring common semantics are identified. Only a few atoms, such as the burger, are not commonalities, as their corresponding images lack sufficient common semantics. The atoms are also repre-

sented accurately. For instance, the atom sets for each image featuring the shark semantic all include the word shark. In the second row (CPE=0.95), our method remains effective in disentangling and describing VC with a higher level of polysemanticity. g identifies a greater variety of atoms. These results demonstrate the effectiveness of the disentanglement and description operation in the CPDF.

4.3. Concept Distribution and CPE

CPE can quantify the polysemanticity and serve as an indicator of a DVM’s interpretability. It begins by calculating the probabilities of each orthogonal atom. As the middle column of Table 1 shows, the distribution provides statistics on the extent to which different atoms are associated with each concept. For instance, concept 75 primarily focuses on blue with a probability of 0.27 while also identifying yellow with a smaller probability. The semantics between atoms are non-overlapping. This probabilistic approach enhances explainability by capturing multiple semantics with their occurring probabilities, upgrading the modeling of deterministic concepts to uncertain atom distributions.

CPE quantifies polysemanticity from 3 levels of granularity. As shown in Fig. 3a, concepts exhibit varying degrees of polysemanticity, with considerable fluctuations (ranging from a maximum of 1 to a minimum of 0.5). Most of the concepts demonstrate a noticeable level of polysemanticity. When analyzing the polysemanticity of different

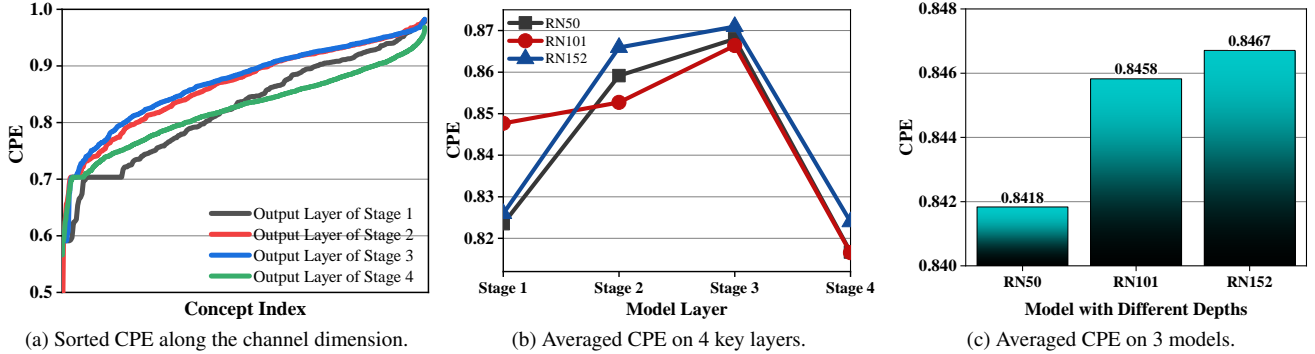


Figure 3. Illustrations of CPE scores at 3 levels of granularity. In (a), the channel indices of each layer are max normalized to 1.

Table 2. The consistency of the recognition of concept polysemanticity between the CPE metric and human scorers.

	Consistency
CPE Metric and Human Scorers	75 %

layers, as shown in Fig. 3b, the averaged CPE peaks in the third stage, while the shallowest and deepest layers exhibit lower values. Typically, deeper layers capture abstract concepts, whereas the shallower layers extract elementary features like textures [69, 74]. DVMs show better monosemanticity when identifying elementary and abstract concepts, while more ambiguous concepts are captured in the intermediate layers. This experiment validates the theoretical and experimental claims of previous work [18, 41]. In Fig. 3c, we observe that as the number of layers increases, the CPE of the model shows a rising trend. This result indicates a direct proportional relationship between the polysemanticity and the complexity of DVMs, which is that the more complex a DVM becomes, the harder it is to interpret.

The CPE is evaluated in comparison with human assessments. As shown in Table 1, the CPE is consistent with the degree of polysemanticity from the human intuitive observations (the polysemanticity of the first row is smaller than that of the second row). Similarly, we randomly sample 300 pairs of VCs, each containing two VCs with varying levels of polysemanticity. Comparisons are drawn from these 300 pairs by both human evaluators and the CPE metric. As shown in Table 2, results from human assessments and CPE achieve a 75% agreement rate, demonstrating the effectiveness of CPE. Other results are shown in Sec. S4 of the Appendix. All of these results reveal that CPE is effective in quantifying the polysemanticity of concepts and DVMs.

4.4. CoE for Local Explanations

CoE generates local explanations akin to CoT by automatically describing the concept circuit. We set $\alpha = 0.001$ to acknowledge the top relevant VCs, resulting in an average of 3 key VCs per layer. As exemplified in Table 3, given an input image, CoE first outputs whether the prediction of the

DVM is correct and then gives reasons behind this prediction according to the information along the concept circuits. CoE employs an LLM as an engine to infer the logical relationships among concepts, as well as between concepts and the context. It synthesizes all evidence to generate an inductive commentary on the predictions. The explanation chain is presented in a linguistic format, enhancing human understanding. For instance, CoE explains why the DVM incorrectly predicted a tench as a mosquito net: the top activation of mosquito-net-related concepts, rather than those related to fish, misled the decision. Additional instances are shown in Sec. S5 of the Appendix. Overall, CoE effectively captures and elucidates the core decision-making evidence for both correct and incorrect predictions of DVMs.

4.5. Quantitative Evaluation via GPT-4o & Human

We employ GPT-4o and human evaluators to assess the local explanations for 500 and 100 samples randomly selected from the ImageNet Validation dataset [20], respectively. The GPT-4o evaluation is achieved through a carefully designed prompt `prompt-coe-eval`. Explanations generated by three methods are rated according to three explainability metrics: Accuracy, Completeness, and User Interpretability [62]. Each is assigned a three-tier scoring system (2, 1, and 0), with specific criteria defined for each tier, resulting in a total explanation score of 6. Please refer to Sec. S2 and S5 of the Appendix for details.

As shown in Table 4, our CoE approach attains peak performance across all three metrics, achieving total scores of 5.06 and 5.04 in GPT-4o and human evaluations, respectively. The lowest scores (3.14 and 2.62) are obtained on the MILAN ANNOTATION dataset without the ACD and CPDF methods. This dataset was manually annotated, resulting in inaccuracy and insufficiency within concept explanations. Scores increase by 0.11 and 0.72, respectively, with the application of our proposed ACD- $\mathcal{B}_{M,T}$ dataset. The ACD method not only enables the automated disentanglement and description of concept atoms but also enhances their precision and comprehensibility. When the CoE em-

Table 3. Cases of local explanations of CoE. The first row shows the explanation of a correct prediction, and the second row is reversed.





	<p>The model outputs a correct result: black-and-tan coonhound. Specifically, in the shallowest layer, layer 1, channel 88 with a relevance value of 1.0 describes the concept curved, which may relate to the curved shapes observed in parts of the dog such as its tail or ears. Moving deeper, in layer 2, channel 506 with a relevance value of 0.85 and channel 391 with a relevance value of 0.75 describe the concept of animal, indicating the model has identified an animal in the image, and channel 229 with a relevance value of 0.77 emphasizes the color black, aligning with the black and tan colors of the coonhound. Further, layer 2 also identifies the presence of grass several times (channels 94 and 103), which corresponds to the grassy field described in the image caption. In layer 3, various channels, such as 985, 174, 422, and 13, with high relevance scores, from 0.72 to 1.0, repeatedly identify the color green and the concept grass, firmly establishing the setting of the image. Additionally, channels 11, 787, and 591 in layer 3 enhance the certainty by repeatedly identifying animal and creature, confirming that the subject is an animal. Finally, layer 4 decisively contributes with channels 1354 and 1661, both signifying dog with high relevance values (1.0 and 0.72 respectively), which correctly identifies the animal in the image as a dog.</p>
 <p>label: black-and-tan coonhound predict: black-and-tan coonhound</p>	<p>Given that the model's structured concepts strongly match the description and characteristics noted in the caption and the ground truth label, it is clear why the model outputs the correct result of black-and-tan coonhound.</p>
	<p>The model outputs an incorrect result mosquito net instead of the correct label tench. Specifically, in the shallowest layer 1 of the model, channel 88 with a relevance value of 1.0 describes the concept of smooth, channel 61 with a relevance value of 0.81 describes the concept of green, and channel 111 with a relevance value of 0.72 describes the concept of brown. In the deeper layer 2 of the model, channel 94 with a relevance value of 1.0 describes the concept of water, channel 229 with a relevance value of 0.84 describes the concept of fish, channel 103 with a relevance value of 0.81 also describes the concept of fish, and channel 467 with a relevance value of 0.73 describes the concept of mesh. At layer 3, channel 985 with a relevance value of 1.0 further describes the concept of fish, while channels 894, 122, and 715 with relevance values of 0.83, 0.73, and 0.72, respectively, describe the concept of green, possibly relating to the color of the net. In the deepest layer 4, channel 697 with a relevance value of 1.0 describes the concept of net, channel 1878 with a relevance value of 0.76 describes the concept of baby, and channel 321 with a relevance value of 0.76 represents the concept of hexagon, which could misconstrue the net structure.</p>
 <p>label: tench predict: mosquito net</p>	<p>The prevalence of concepts related to fish within the decision path suggests a relationship to the tench, but the final prediction of mosquito net was likely influenced by the dominance of net-related concepts. Thus, the model was misled by the presence of a net, resulting in the incorrect classification of mosquito net.</p>

Table 4. Scores of CoE for the local explanation on three methods evaluated by GPT-4o and human scorers. The first method utilizes MILAN ANNOTATION as the concept explanation dataset, while the rest two work on the ACD- $\mathcal{B}_{M,T}$ datasets. **Each criterion has a maximum score of 2 points. The total explanation score is 6 points.** Higher scores indicate better explainability.

	Method	Accuracy	Completeness	User Interpret.	Total Explanation
GPT-4o	MILAN A.[35] + Description (Baseline)	1.03	1.07	1.04	3.14
	CoE w/o Filtering	1.07	1.10	1.08	3.25
	CoE (ours)	1.69	1.70	1.67	5.06
Human	MILAN A.[35] + Description (Baseline)	0.87	0.83	0.92	2.62
	CoE w/o Filtering	1.10	1.16	1.07	3.34
	CoE (ours)	1.73	1.72	1.59	5.04

employs the full CPDF mechanism, the explanation score rises by 1.92 and 2.42 points (the average absolute improvement is 36%), respectively, with the filtering step contributing 1.81 and 1.70 points. This result suggests that by taking polysemanticity and contextual filtering of concepts into account, CoE effectively guides the LLM in producing better linguistic explanations, substantially enhancing their accuracy, completeness, and interpretability for users. The results of the human evaluation are consistent with the GPT-4o results. All of these results strongly affirm the superiority of the proposed CoE approach.

5. Conclusion

In this paper, we propose a CoE approach to tackle the challenges of the inflexibility to automatically construct con-

cept explanation datasets, insufficient linguistic explanations, and the weakness in managing concept polysemanticity of concept-based XAI methods. CoE automates the decoding and description of concepts via an LVLm and constructs global concept explanation datasets. A CPDF mechanism is designed to identify the most contextually relevant concept atoms, advancing the modeling of deterministic concepts to uncertain concept atom distributions. The CPE is proposed to quantify the polysemanticity. Finally, CoE enables local explanations of a DVM's decision-making process, represented through natural language. The effectiveness and superiority of CPE and CoE are demonstrated. In summary, CoE establishes a systematical framework for explaining DVMs, and we believe that the findings presented in this paper warrant further exploration.

Acknowledgment

This research is supported in part by the National Natural Science Foundation of China under Grants U23B2049, 62276186, and 61925602.

References

- [1] Josh Achiam, Steven Adler, Sandhini Agarwal, Lama Ahmad, Ilge Akkaya, Florencia Leoni Aleman, Diogo Almeida, Janko Altmenschmidt, Sam Altman, Shyamal Anadkat, et al. Gpt-4 technical report. *arXiv preprint arXiv:2303.08774*, 2023. 5
- [2] Reduan Achtibat, Maximilian Dreyer, Ilona Eisenbraun, Sebastian Bosse, Thomas Wiegand, Wojciech Samek, and Sebastian Lapuschkin. From attribution maps to human-understandable explanations through concept relevance propagation. *Nature Machine Intelligence*, 5(9):1006–1019, 2023. 5, 6
- [3] Reduan Achtibat, Maximilian Dreyer, Ilona Eisenbraun, Sebastian Bosse, Thomas Wiegand, Wojciech Samek, and Sebastian Lapuschkin. From attribution maps to human-understandable explanations through concept relevance propagation. *Nature Machine Intelligence*, 5(9):1006–1019, 2023. 1, 2, 5
- [4] Reduan Achtibat, Sayed Mohammad Vakilzadeh Hatefi, Maximilian Dreyer, Aakriti Jain, Thomas Wiegand, Sebastian Lapuschkin, and Wojciech Samek. Attnlrp: attention-aware layer-wise relevance propagation for transformers. In *Proceedings of the 41st International Conference on Machine Learning*, pages 135–168, 2024. 9
- [5] Rajaram Achyuta, Chowdhury Neil, Torralba Antonio, Andreas Jacob, and Schwettmann Sarah. Automatic discovery of visual circuits. In *NeurIPS Workshop on Attributing Model Behavior at Scale*, 2023. 1, 2, 5
- [6] Sebastian Bach, Alexander Binder, Grégoire Montavon, Frederick Klauschen, Klaus-Robert Müller, and Wojciech Samek. On pixel-wise explanations for non-linear classifier decisions by layer-wise relevance propagation. *PLoS ONE*, 10, 2015. 1
- [7] David Bau, Jun-Yan Zhu, Hendrik Strobelt, Agata Lapedriza, Bolei Zhou, and Antonio Torralba. Understanding the role of individual units in a deep neural network. *Proceedings of the National Academy of Sciences*, 117(48):30071–30078, 2020. 2
- [8] Leonard Bereska and Efstratios Gavves. Mechanistic interpretability for ai safety—a review. *arXiv preprint arXiv:2404.14082*, 2024. 1
- [9] Subrato Bharati, M Rubaiyat Hossain Mondal, and Prajyo Podder. A review on explainable artificial intelligence for healthcare: why, how, and when? *IEEE Transactions on Artificial Intelligence*, 2023. 1
- [10] Moritz Böhle, Navdeep Singh, Mario Fritz, and Bernt Schiele. B-cos alignment for inherently interpretable cnns and vision transformers. *IEEE Transactions on Pattern Analysis and Machine Intelligence*, 46(6):4504–4518, 2024. 2
- [11] Zhe Chen, Weiyun Wang, Hao Tian, Shenglong Ye, Zhangwei Gao, Erfei Cui, Wenwen Tong, Kongzhi Hu, Jiapeng Luo, Zheng Ma, et al. How far are we to gpt-4v? closing the gap to commercial multimodal models with open-source suites. *arXiv preprint arXiv:2404.16821*, 2024. 4
- [12] Zhe Chen, Jiannan Wu, Wenhai Wang, Weijie Su, Guo Chen, Sen Xing, Muyan Zhong, Qinglong Zhang, Xizhou Zhu, Lewei Lu, et al. Internvl: Scaling up vision foundation models and aligning for generic visual-linguistic tasks. In *Proceedings of the IEEE/CVF Conference on Computer Vision and Pattern Recognition*, pages 24185–24198, 2024. 4
- [13] Ming-Ming Cheng, Peng-Tao Jiang, Ling-Hao Han, Liang Wang, and Philip Torr. Deeply explain cnn via hierarchical decomposition. *International Journal of Computer Vision*, 131(5):1091–1105, 2023. 2
- [14] Mehdi Cherti, Romain Beaumont, Ross Wightman, Mitchell Wortsman, Gabriel Ilharco, Cade Gordon, Christoph Schuhmann, Ludwig Schmidt, and Jenia Jitsev. Reproducible scaling laws for contrastive language-image learning. In *Proceedings of the IEEE/CVF Conference on Computer Vision and Pattern Recognition*, pages 2818–2829, 2023. 6
- [15] Zheng Chu, Jingchang Chen, Qianglong Chen, Weijiang Yu, Tao He, Haotian Wang, Weihua Peng, Ming Liu, Bing Qin, and Ting Liu. A survey of chain of thought reasoning: Advances. *Frontiers and Future*, 2023. 4
- [16] Zheng Chu, Jingchang Chen, Qianglong Chen, Weijiang Yu, Tao He, Haotian Wang, Weihua Peng, Ming Liu, Bing Qin, and Ting Liu. Navigate through enigmatic labyrinth a survey of chain of thought reasoning: Advances, frontiers and future. In *Proceedings of the 62nd Annual Meeting of the Association for Computational Linguistics (Volume 1: Long Papers)*, pages 1173–1203, 2024. 5
- [17] Arthur Conmy, Augustine Mavor-Parker, Aengus Lynch, Stefan Heimersheim, and Adrià Garriga-Alonso. Towards automated circuit discovery for mechanistic interpretability. *Advances in Neural Information Processing Systems*, 36: 16318–16352, 2023. 2
- [18] Meghal Dani, Isabel Rio-Torto, Stephan Alaniz, and Zeynep Akata. Devil: Decoding vision features into language. In *DAGM German Conference on Pattern Recognition*, pages 363–377. Springer, 2023. 1, 4, 7
- [19] Jia Deng, Wei Dong, Richard Socher, Li-Jia Li, Kai Li, and Li Fei-Fei. Imagenet: A large-scale hierarchical image database. In *2009 IEEE conference on Computer Vision and Pattern Recognition*, pages 248–255. Ieee, 2009. 6
- [20] Jia Deng, Wei Dong, Richard Socher, Li-Jia Li, Kai Li, and Li Fei-Fei. Imagenet: A large-scale hierarchical image database. In *2009 IEEE conference on computer vision and pattern recognition*, pages 248–255. Ieee, 2009. 7
- [21] Maximilian Dreyer, Erblina Purlku, Johanna Vielhaben, Wojciech Samek, and Sebastian Lapuschkin. Pure: Turning polysemantic neurons into pure features by identifying relevant circuits. In *Proceedings of the IEEE/CVF Conference on Computer Vision and Pattern Recognition (CVPR) Workshops*, pages 8212–8217, 2024. 1, 2, 3
- [22] Nelson Elhage, Neel Nanda, Catherine Olsson, Tom Henighan, Nicholas Joseph, Ben Mann, Amanda Askell, Yuntao Bai, Anna Chen, Tom Conerly, et al. A mathematical framework for transformer circuits. *Transformer Circuits Thread*, 1(1):12, 2021. 2

- [23] Nelson Elhage, Tristan Hume, Catherine Olsson, Nicholas Schiefer, Tom Henighan, Shauna Kravec, Zac Hatfield-Dodds, Robert Lasenby, Dawn Drain, Carol Chen, et al. Toy models of superposition. *arXiv preprint arXiv:2209.10652*, 2022. 3
- [24] Sebastian Farquhar, Jannik Kossen, Lorenz Kuhn, and Yarin Gal. Detecting hallucinations in large language models using semantic entropy. *Nature*, 630(8017):625–630, 2024. 4
- [25] Thomas Fel, Victor Boutin, Louis Béthune, Rémi Cadène, Mazda Moayeri, Léo Andéol, Mathieu Chalvidal, and Thomas Serre. A holistic approach to unifying automatic concept extraction and concept importance estimation. *Advances in Neural Information Processing Systems*, 36, 2024. 2, 3
- [26] Guhao Feng, Bohang Zhang, Yuntian Gu, Haotian Ye, Di He, and Liwei Wang. Towards revealing the mystery behind chain of thought: a theoretical perspective. *Advances in Neural Information Processing Systems*, 36, 2024. 4
- [27] Guhao Feng, Bohang Zhang, Yuntian Gu, Haotian Ye, Di He, and Liwei Wang. Towards revealing the mystery behind chain of thought: a theoretical perspective. *Advances in Neural Information Processing Systems*, 36, 2024. 2, 4
- [28] Yossi Gandelsman, Alexei A. Efros, and Jacob Steinhardt. Interpreting clip’s image representation via text-based decomposition. In *The Twelfth International Conference on Learning Representations*, 2024. 4
- [29] Amirata Ghorbani, James Wexler, James Y Zou, and Been Kim. Towards automatic concept-based explanations. *Advances in neural information processing systems*, 32, 2019. 1, 2
- [30] Dan W Grupe and Jack B Nitschke. Uncertainty and anticipation in anxiety: an integrated neurobiological and psychological perspective. *Nature Reviews Neuroscience*, 14(7): 488–501, 2013. 2
- [31] Kaiming He, Xiangyu Zhang, Shaoqing Ren, and Jian Sun. Deep residual learning for image recognition. In *Proceedings of the IEEE conference on Computer Vision and Pattern Recognition*, pages 770–778, 2016. 6
- [32] Kaiming He, Xiangyu Zhang, Shaoqing Ren, and Jian Sun. Deep residual learning for image recognition. In *Proceedings of the IEEE conference on Computer Vision and Pattern Recognition*, pages 770–778, 2016. 5
- [33] Pengcheng He, Xiaodong Liu, Jianfeng Gao, and Weizhu Chen. DeBERTa: Decoding-enhanced bert with disentangled attention. In *International Conference on Learning Representations*, 2020. 4
- [34] Evan Hernandez, Sarah Schwettmann, David Bau, Teona Bagashvili, Antonio Torralba, and Jacob Andreas. Natural language descriptions of deep features. In *International Conference on Learning Representations*, 2022. 5, 6
- [35] Evan Hernandez, Sarah Schwettmann, David Bau, Teona Bagashvili, Antonio Torralba, and Jacob Andreas. Natural language descriptions of deep features. In *International Conference on Learning Representations*, 2022. 1, 2, 4, 8
- [36] Been Kim, Martin Wattenberg, Justin Gilmer, Carrie Cai, James Wexler, Fernanda Viegas, et al. Interpretability beyond feature attribution: Quantitative testing with concept activation vectors (tcav). In *International conference on machine learning*, pages 2668–2677. PMLR, 2018. 1, 3
- [37] Anton Kuznetsov, Balint Gyevnar, Cheng Wang, Steven Peters, and Stefano V. Albrecht. Explainable ai for safe and trustworthy autonomous driving: A systematic review. *IEEE Transactions on Intelligent Transportation Systems*, pages 1–23, 2024. 1
- [38] Yann LeCun, Yoshua Bengio, and Geoffrey Hinton. Deep learning. *nature*, 521(7553):436–444, 2015. 1
- [39] Junnan Li, Dongxu Li, Silvio Savarese, and Steven Hoi. Blip-2: Bootstrapping language-image pre-training with frozen image encoders and large language models. In *International conference on machine learning*, pages 19730–19742. PMLR, 2023. 4
- [40] Haomiao Liu, Ruiping Wang, Shiguang Shan, and Xilin Chen. What is a tabby? interpretable model decisions by learning attribute-based classification criteria. *IEEE transactions on pattern analysis and machine intelligence*, 43(5): 1791–1807, 2019. 2
- [41] Francesco Locatello, Stefan Bauer, Mario Lucic, Gunnar Raetsch, Sylvain Gelly, Bernhard Schölkopf, and Olivier Bachem. Challenging common assumptions in the unsupervised learning of disentangled representations. In *international conference on machine learning*, pages 4114–4124. PMLR, 2019. 7
- [42] Simon C Marshall and Jan H Kirchner. Understanding polysemanticity in neural networks through coding theory. *arXiv preprint arXiv:2401.17975*, 2024. 2, 3
- [43] Dang Minh, H Xiang Wang, Y Fen Li, and Tan N Nguyen. Explainable artificial intelligence: a comprehensive review. *Artificial Intelligence Review*, pages 1–66, 2022. 1
- [44] Grégoire Montavon, Sebastian Lapuschkin, Alexander Binder, Wojciech Samek, and Klaus-Robert Müller. Explaining nonlinear classification decisions with deep taylor decomposition. *Pattern recognition*, 65:211–222, 2017. 2
- [45] Grégoire Montavon, Alexander Binder, Sebastian Lapuschkin, Wojciech Samek, and Klaus-Robert Müller. Layer-wise relevance propagation: an overview. *Explainable AI: interpreting, explaining and visualizing deep learning*, pages 193–209, 2019. 4
- [46] Grégoire Montavon, Alexander Binder, Sebastian Lapuschkin, Wojciech Samek, and Klaus-Robert Müller. Layer-wise relevance propagation: an overview. *Explainable AI: interpreting, explaining and visualizing deep learning*, pages 193–209, 2019. 1, 2
- [47] Meike Nauta, Ron van Bree, and Christin Seifert. Neural prototype trees for interpretable fine-grained image recognition. In *Proceedings of the IEEE/CVF Conference on Computer Vision and Pattern Recognition (CVPR)*, pages 14933–14943, 2021. 2
- [48] Tuomas Oikarinen and Tsui-Wei Weng. Clip-dissect: Automatic description of neuron representations in deep vision networks. *arXiv preprint arXiv:2204.10965*, 2022. 9
- [49] Laura O’Mahony, Vincent Andrearczyk, Henning Müller, and Mara Graziani. Disentangling neuron representations with concept vectors. In *Proceedings of the IEEE/CVF Conference on Computer Vision and Pattern Recognition*, pages 3770–3775, 2023. 3

- [50] OpenAI. Hello gpt-4o. <https://openai.com/index/hello-gpt-4o/>, 2024. 4
- [51] Alec Radford, Jong Wook Kim, Chris Hallacy, Aditya Ramesh, Gabriel Goh, Sandhini Agarwal, Girish Sastry, Amanda Askell, Pamela Mishkin, Jack Clark, et al. Learning transferable visual models from natural language supervision. In *International Conference on Machine Learning*, pages 8748–8763. PMLR, 2021. 6
- [52] Alec Radford, Jong Wook Kim, Chris Hallacy, Aditya Ramesh, Gabriel Goh, Sandhini Agarwal, Girish Sastry, Amanda Askell, Pamela Mishkin, Jack Clark, et al. Learning transferable visual models from natural language supervision. In *International conference on machine learning*, pages 8748–8763. PMLR, 2021. 5
- [53] Yao Rong, Tobias Leemann, Thai-Trang Nguyen, Lisa Fiedler, Peizhu Qian, Vaibhav Unhelkar, Tina Seidel, Gjergji Kasneci, and Enkelejda Kasneci. Towards human-centered explainable ai: A survey of user studies for model explanations. *IEEE transactions on pattern analysis and machine intelligence*, 46(4):2104–2122, 2024. 1
- [54] Cynthia Rudin. Stop explaining black box machine learning models for high stakes decisions and use interpretable models instead. *Nature Machine Intelligence*, 1(5):206–215, 2019. 2
- [55] Waddah Saeed and Christian Omlin. Explainable ai (xai): A systematic meta-survey of current challenges and future opportunities. *Knowledge-Based Systems*, 263:110273, 2023. 1, 2
- [56] Pranab Sahoo, Ayush Kumar Singh, Sriparna Saha, Vinija Jain, Samrat Mondal, and Aman Chadha. A systematic survey of prompt engineering in large language models: Techniques and applications. *arXiv preprint arXiv:2402.07927*, 2024. 5
- [57] Christoph Schuhmann, Romain Beaumont, Richard Vencu, Cade W Gordon, Ross Wightman, Mehdi Cherti, Theo Coombes, Aarush Katta, Clayton Mullis, Mitchell Wortsman, Patrick Schramowski, Srivatsa R Kundurthy, Katherine Crowson, Ludwig Schmidt, Robert Kaczmarczyk, and Jenia Jitsev. LAION-5b: An open large-scale dataset for training next generation image-text models. In *Thirty-sixth Conference on Neural Information Processing Systems Datasets and Benchmarks Track*, 2022. 6
- [58] Ramprasaath R Selvaraju, Michael Cogswell, Abhishek Das, Ramakrishna Vedantam, Devi Parikh, and Dhruv Batra. Grad-cam: Visual explanations from deep networks via gradient-based localization. In *Proceedings of the IEEE international conference on computer vision (ICCV)*, pages 618–626, 2017. 1, 2
- [59] Ao Sun, Pingchuan Ma, Yuanyuan Yuan, and Shuai Wang. Explain any concept: Segment anything meets concept-based explanation. *Advances in Neural Information Processing Systems*, 36, 2024. 4
- [60] Ao Sun, Pingchuan Ma, Yuanyuan Yuan, and Shuai Wang. Explain any concept: Segment anything meets concept-based explanation. *Advances in Neural Information Processing Systems*, 36, 2024. 1, 2
- [61] Giulia Vilone and Luca Longo. Notions of explainability and evaluation approaches for explainable artificial intelligence. *Information Fusion*, 76:89–106, 2021. 8
- [62] Giulia Vilone and Luca Longo. Notions of explainability and evaluation approaches for explainable artificial intelligence. *Information Fusion*, 76:89–106, 2021. 7
- [63] Kevin Ro Wang, Alexandre Variengien, Arthur Conmy, Buck Shlegeris, and Jacob Steinhardt. Interpretability in the wild: a circuit for indirect object identification in GPT-2 small. In *The Eleventh International Conference on Learning Representations, ICLR 2023, Kigali, Rwanda, May 1-5, 2023*. 2
- [64] Teng Wang, Jinrui Zhang, Junjie Fei, Hao Zheng, Yunlong Tang, Zhe Li, Mingqi Gao, and Shanshan Zhao. Caption anything: Interactive image description with diverse multimodal controls. *arXiv preprint arXiv:2305.02677*, 2023. 4
- [65] Xiaosong Wang, Yifan Peng, Le Lu, Zhiyong Lu, Mohammadhadi Bagheri, and Ronald M Summers. Chestx-ray8: Hospital-scale chest x-ray database and benchmarks on weakly-supervised classification and localization of common thorax diseases. In *Proceedings of the IEEE conference on computer vision and pattern recognition*, pages 2097–2106, 2017. 9
- [66] Xin Wang, Hong Chen, Si’ao Tang, Zihao Wu, and Wenwu Zhu. Disentangled representation learning. *IEEE Transactions on Pattern Analysis and Machine Intelligence*, 46(12):9677–9696, 2024. 1
- [67] Jason Wei, Xuezhi Wang, Dale Schuurmans, Maarten Bosma, Fei Xia, Ed Chi, Quoc V Le, Denny Zhou, et al. Chain-of-thought prompting elicits reasoning in large language models. *Advances in neural information processing systems*, 35:24824–24837, 2022. 2, 4
- [68] Hongxu Yin, Pavlo Molchanov, Jose M Alvarez, Zhizhong Li, Arun Mallya, Derek Hoiem, Niraj K Jha, and Jan Kautz. Dreaming to distill: Data-free knowledge transfer via deep-inversion. In *Proceedings of the IEEE/CVF conference on computer vision and pattern recognition (CVPR)*, pages 8715–8724, 2020. 1
- [69] Wenlong Yu, Ruonan Liu, Dongyue Chen, and Qinghua Hu. Explainability enhanced object detection transformer with feature disentanglement. *IEEE Transactions on Image Processing*, 33:6439–6454, 2024. 7
- [70] Yu Zhang, Peter Tiño, Aleš Leonardis, and Ke Tang. A survey on neural network interpretability. *IEEE Transactions on Emerging Topics in Computational Intelligence*, 5(5):726–742, 2021. 2
- [71] Shitian Zhao, Zhuowan Li, Yadong Lu, Alan Yuille, and Yan Wang. Causal-cog: A causal-effect look at context generation for boosting multi-modal language models. In *Proceedings of the IEEE/CVF Conference on Computer Vision and Pattern Recognition (CVPR)*, pages 13342–13351, 2024. 2
- [72] Bolei Zhou, Aditya Khosla, Agata Lapedriza, Aude Oliva, and Antonio Torralba. Learning deep features for discriminative localization. In *2016 IEEE Conference on Computer Vision and Pattern Recognition (CVPR)*, pages 2921–2929, 2016. 5
- [73] Bolei Zhou, Agata Lapedriza, Aditya Khosla, Aude Oliva, and Antonio Torralba. Places: A 10 million image database for scene recognition. *IEEE transactions on pattern analysis and machine intelligence*, 40(6):1452–1464, 2017. 9

- [74] Bolei Zhou, David Bau, Aude Oliva, and Antonio Torralba. Interpreting deep visual representations via network dissection. *IEEE transactions on pattern analysis and machine intelligence*, 41(9):2131–2145, 2018. [2](#), [3](#), [7](#)

CoE: Chain-of-Explanation via Automatic Visual Concept Circuit Description and Polysemanticity Quantification

Supplementary Material

Contents

S1. Overview of Supplementary Material	1
S2. Prompt Engineering	1
S2.1. Prompt for Commonality Describing	1
S2.2. Prompt for CoE Local Explanation	2
S2.3. Prompt for Evaluating Local Explanations .	3
S3. Details of the CoE Approach	3
S3.1. Probability of Concept Atoms and CPE . .	3
S3.2. Explanation of the Concept	4
S3.3. Discussion Between CoE and CoT	4
S3.4. Time and Cost of CoE	4
S4. Experiments on CPE	4
S4.1. Various Versions of CPE	4
S4.2. Different XAI Methods	5
S4.3. Different Model Architectures	6
S4.4. Human Evaluation on CPE	6
S4.5. Examples of Disentanglement and CPE . .	8
S5. Experiments on CoE Local Explanations	8
S5.1. Evaluation of Local Explanations	8
S5.2. Supplemental Quantitative Evaluation Results	9
S5.3. Examples of CoE Local Explanations . . .	9
S5.4. Comparison Between CoE and Baseline . .	10

S1. Overview of Supplementary Material

In this supplementary material, we mainly give detailed information and analyses about prompt engineering, the CoE approach, and experimental results of the CPE and CoE local explanations. Specifically, as presented in Sec. S2, the prompts that are well-designed in this paper include `prompt-com` for automatically disentangling and describing the commonalities of the given VCs, `prompt-coe` for generating the local explanations given specific samples, and `prompt-coe-eval` for evaluating the local explanations from three explainability metrics. In Sec. S3, we present details of the CoE approach, highlighting its distinguishing qualities. We also discuss the distinctions between CoE and CoT. In Sec. S4, we give experimental results of various versions of CPE, including naive CPE, CPE with clustering, and our final refined version. We also analyze the CPE results explored from different XAI methods (i.e., relevance, activation, and maximum mutual information-based methods) and different model architectures (i.e., ResNet and CLIP). Various examples of VCs,

Table S5. The prompt template of `prompt-com`. Before querying the LVLMs, we substitute the curly brackets with actual texts.

```
Prompt for Commonality Disentanglement and Description

[System:]
You are a helpful assistant designed to describe the commonality and specificity of the given images, and output a JSON format response.

[User:]
Given {N} images, each containing highlighted regions, find some common objects and attributes in these images and describe each image with words especially repeated across these images.

Your response should follow these rules:
{Rules}

Your identification process should follow these steps: {CoT Steps}

Now, please provide your response:
{Response}
```

their disentangled concept atoms, probabilities, and CPE values are provided. Besides, we give details on the implementation of the comparison experiments between human evaluations and the CPE metric. In the Section S5, we provide details of the evaluation criteria for linguistic local explanations, along with an overview of the human evaluation process. Details of the comparison between local linguistic explanations generated by different methods and various instances of these local explanations are presented.

S2. Prompt Engineering

In this section, we provide a detailed exposition of the three well-engineered prompts designed to describe commonalities of VCs, aggregate all information along the concept circuit to enable the CoE to generate local explanations and evaluate the generated local explanations.

S2.1. Prompt for Commonality Describing

In this paper, we design a sophisticated prompt `prompt-com` to describe the commonalities by a set of concept atoms. The meticulously crafted prompt template is presented in Table S5. As discussed in the main manuscript, this prompt is engineered to accurately

disentangle and summarize the commonalities across multiple subsets of images utilizing precise terminology drawn from 13 semantic directions. Additionally, the disentangled atoms also serve as the foundation for the probability and CPE calculations. To meet these requirements, this prompt incorporates some rules along with step-by-step guidance. The rules outlined below primarily establish 13 semantic directions and delineate the format for output control.

1. Pay more attention to the repeated objects or attributes across these images.
2. Possible objects or attributes you can use to describe these images are object category, scene, object part, color, texture, material, position, transparency, brightness, shape, size, edges, and their relationships.
3. The identified common objects or attributes must appear simultaneously in at least 5 images.
4. The identified specific objects or attributes represent some important contents of an individual image but not in the common objects or attributes found in the previous step.
5. Your description of each image should be simple and only 3 words.
6. Your response should be in the format of a JSON file, of which each key is a simple image index and each value is an object or attribute.

To enhance the quality of disentanglement and description of atoms, this task is structured into three steps, drawing inspiration from the CoT method.

Step 1, take an overview of all 15 images and summarize all possible common objects or attributes that appear simultaneously in at least any 5 of these images.

Step 2, for each individual image, identify the common objects or attributes found in Step 1 that also appear in the current image to describe the current image.

Step 3, for each individual image, you can also use some specific attributes or objects that are not common across these images to describe the current image if there is not enough 3-word description for the common object or attribute found in Step 2.

Table S6. The prompt template of `prompt-coe`. Before querying the LLMs, we substitute the curly brackets with actual texts.

Prompt for CoE Local Explanations
<pre>[System:] You are an intelligent deep learning model explainer and you are now explaining the decision predicted by a deep vision identification model. [User:] Given a prediction of a deep vision model and its prediction path formulated in the format of a concept circuit, you should first judge whether the model prediction is correct or incorrect and then give the reason why the prediction is correct or incorrect based on the following pieces of information (A, B, C, D, E). You should generate an aggregated and rigorous paragraph based on the given information rather than imagination. The information: {A, B, C, D, E} There are some rules for your response: {Rules} Positive and negative prediction examples are given: {Positive Example}, {Negative Example} Your inference process should follow these steps: {CoT Steps} Now, please provide your response: {Response}</pre>

S2.2. Prompt for CoE Local Explanation

In this paper, we design a prompt `prompt-coe` for the LLM to aggregate all information along the concept circuit and generate a local explanation chain to explain the decision-making process of a DVM. This explanation chain is similar to CoT in terms of the structure of the output. The prompt template is presented in Table S6. The information provided in this prompt includes the DVM’s prediction, sample label, image caption, relevant concept explanations derived by applying the CPDF mechanism on the automatically constructed $ACD-B_{M,T}$ dataset, and their corresponding relevance values. The concept explanations and relevance values are presented in a structured format.

In this prompt, the rule set primarily functions to regulate the output. Furthermore, we develop two examples of local explanations based on few-shot prompting: a positive example, wherein the CoE generates local explanations corresponding to a correct prediction of the DVM, and a negative example, illustrating the expected local explanation.

tion when the DVM prediction is incorrect. Likewise, the process of CoE generating local explanations adheres to the CoT method, as detailed below.

Step 1, Based on information A), which is the model’s prediction, and information B, which is the ground truth label of the input image, You first need to determine whether the two are semantically equivalent. If they are semantically equivalent, then the model’s prediction is considered correct. If the prediction and the label are not semantically equivalent, it is considered an incorrect prediction.

Step 2, Based on the judgment in Step 1 and the given information C, D, and E, which include the caption of the input image, the vision model’s decision path and the concept information at each node along the path, and the concept relevance values at each node, you need to explain why the model arrived at this correct or incorrect prediction. Analyze the decision process by examining each concept in the decision path to determine how they contributed to the final outcome.

S2.3. Prompt for Evaluating Local Explanations

It is essential to evaluate the generated linguistic local explanations utilizing LVLMs. As illustrated in Table S7, to ensure rigor and precision, we meticulously design a prompt `prompt-coe-eval`, which primarily comprises four components: key information, evaluation criteria, evaluation steps, and rules. The key information includes the image, prediction, label, and the generated local explanations. The three explainability evaluation criteria—Accuracy, Completeness, and User Interpretability—are discussed in detail in Sec. S5.1. Each criterion follows a three-level scoring system (2, 1, 0). These scoring guidelines are explicitly conveyed to the LVLM. The explanation process also adheres to the CoT method, requiring the LVLM to first output the scores alongside evidence and then aggregate these into a final score, as outlined below.

Please first provide evidence of your evaluation for each criterion and then provide your score for each criterion, avoiding any potential bias and ensuring that the order in which the responses were presented does not affect your judgment.

Table S7. The prompt template of `prompt-coe-eval`. Before querying the LVLMs, curly brackets are filled with actual texts.

Prompt for Evaluating CoE Local Explanations
<pre>[System:] You are now a scorer for an interpretability evaluation system assessing a deep visual model interpreter. [User:] This interpreter provides natural language explanations of the decision-making process of a deep visual model when given an image input. Your task is to evaluate and score the output explanation of the interpreter based on specified criteria to determine its quality. Your input information includes: {A, B, C, D} Based on the four pieces of information provided above, score Explanation D according to the following three criteria. Each Criteria has its own scoring rules, and you need to score Explanation D according to the standards of each Criteria: {Criteria} CoT Steps for This Prompt: {CoT Steps} Output Control: {Rules} Now, Please provide your response: {Response}</pre>

Then sum up the above scores of the three criteria as the total score.

Finally, output the evidence and scores for these criteria.

S3. Details of the CoE Approach

In this section, we present supplementary details of the CoE approach, including the formulations of the CPE and the distinction from CoT.

S3.1. Probability of Concept Atoms and CPE

In this paper, we acquire the probability of concept atoms by calculating their frequency of occurrence in the disen-

tangled concept atom set \mathcal{A} , given a fixed parameter Q and N . The naive version of probability of i_{th} atom is

$$p_i^{Naive} = \frac{Num_i}{Q \times N}. \quad (13)$$

Accordingly, the naive CPE of j_{th} concept can be formulated as

$$H_j^{Naive} = \frac{-\sum_{i=1}^Q p_i^{Naive} \log p_i^{Naive}}{\log(Q)}. \quad (14)$$

As the CPE proposed in this paper serves as an indicator of the interpretability of concepts and DVMs, we normalize the entropy value to a range between 0 and 1 by dividing it by the logarithm of the number total of atoms.

We cluster the atoms in \mathcal{A} , as some disentangled atoms are semantically equivalent. The probability and CPE of the clustered atoms in \mathcal{A}^* are formulated as

$$p_i^{Cluster} = \frac{Num_i}{Q \times N}, \quad (15)$$

$$H_j^{Cluster} = \frac{-\sum_{i=1}^{P^*} p_i^{Cluster} \log p_i^{Cluster}}{\log(P^*)}. \quad (16)$$

However, there exists a case in which this CPE evaluation becomes ineffective, i.e., when all image patches of a VC are highly similar, as exemplified in the first row of Table S8. The concept should ideally exhibit monosemanticity in this scenario. In contrast, the CPE calculated by Eq. 16 results in a value of 1, as the probabilities of all atoms are evenly distributed (e.g., each with a probability of $1/3$ when $P^* = 3$). To mitigate this problem, we set the minimum number of concept atoms in \mathcal{A}^* to N , assuming that each VC contains at least N common atoms. The padding atoms (in a number of $Pad = N - P^*$) are each assigned a frequency of 1. This operation preserves the relative probabilities among the P^* atoms, ensuring that more frequent atoms remain prevalent while less frequent ones retain their lower counts. Upon completion of these procedures, the probability and CPE are updated to Eq. 8 and Eq. 9 in the main manuscript. The experiments are conducted in Sec. S4.1, showing the effectiveness of our method.

S3.2. Explanation of the Concept

In this paper, we define each channel or neuron of DNNs as a VC, represented by a set of masked image patches [28, 45]. Notably, some works consider each image patch as a VC [59], resembling a form of pixel-level semantic segmentation. Channel-based interpretation can serve as both global and local explanations for a DVM by decoding and describing the commonalities among a set of image patches. It better represents the decision concepts learned internally by the DVM. In contrast, the latter, identifying the key regions within a given image, only serves as a local explanation. Our CoE approach can automatically describe these two directions, as both take the form of image patches.

S3.3. Discussion Between CoE and CoT

The CoE approach proposed in this paper draws inspiration from CoT [15, 26], yet with notable distinctions. CoT directly guides large-scale models to articulate their decision-making processes through carefully crafted prompts. However, it has the following limitations: 1. Each step in the CoT still relies on the large model’s own capabilities, and each prediction of the current step remains unexplained; 2. CoT mainly emerges in LLMs or LVLMs, whereas the capability for smaller DVMs is insufficient. In contrast, CoE dissects the DVMs by identifying critical decision concepts within key layers. These concepts, described in natural language, serve as nodes in a chain. CoE aggregates these nodes to form a coherent explanation chain that elucidates the DVM’s decision-making process. Although the output structure resembles that of CoT, the construction of the CoE explanation chain is achieved by leveraging the general capabilities of LVLMs to automatically describe the VCs and construct the explanation chains. Additionally, CoE provides global conceptual explanations for DVMs while also possessing the capability to quantify polysemanticity. Thus, CoE and CoT are notably distinct.

S3.4. Time and Cost of CoE

CoE primarily consists of ACD, CPE, CPDF, and local explanation steps. ACD and CPE can be performed offline and obtained through a one-off computation process. Building the global ACD- \mathcal{B} database on ImageNet-val takes 9 hours and costs \$70. After that, online inference for the local explanation of a single image requires 20 seconds and costs \$0.01. Compared to manual labor, this cost is considered acceptable.

S4. Experiments on CPE

In this section, we provide additional experiments across various versions of CPE, XAI methods, model architectures, and illustrative examples of CPE.

S4.1. Various Versions of CPE

The proposed CPE has evolved through three iterations: the naive version (Eq. 13 and Eq. 14), the clustered version (Eq. 15 and Eq. 16), and the final refined version (Eq. 8 and Eq. 9 in the main manuscript). As shown in Fig. S4, some atoms disentangled for a single concept are semantically equivalent (e.g., barrier and fence, entry and gate), and many of them exhibit low probabilities. After clustering through the entailment model, all semantically redundant atoms are consolidated, leading to adjusted atom probabilities and a reduced CPE value. The semantics of the atoms are mutually exclusive. For a ResNet152 model, 3.5 atoms per concept, on average, are reduced, as illustrated in Fig. S5. Notably, in the third stage, where polysemanticity

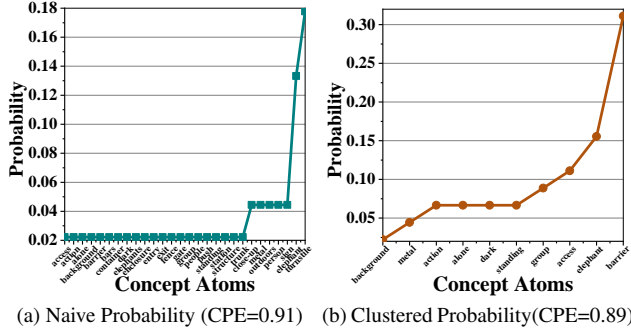


Figure S4. Examples of two versions of the disentangled concept atom probability distributions. (a) shows the naive version, while (b) represents the clustered one. The channel showed here is number 163 of the output layer of Stage 4 of a ResNet152 model.

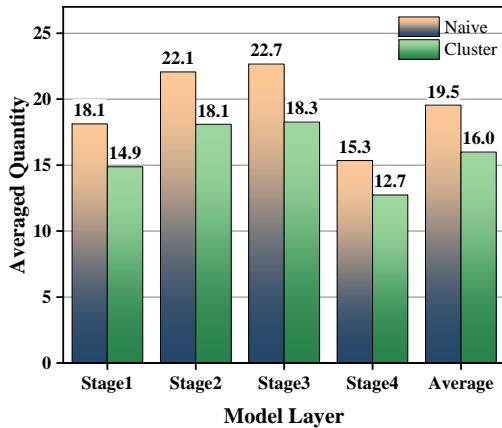


Figure S5. Averaged quantity of disentangled concept atoms. The average term is the averaged quantity of 4 stages.

is most pronounced, the largest reduction is observed, averaging 4.4 per concept. This highlights the significance of introducing the entailment model within the CPDF mechanism to cluster redundant semantics.

Furthermore, as shown in Fig. S5, it is evident that concepts of DVMs exhibit polysemanticity, with the fewest distinct semantics occurring at the final layer (an average of 12.7 non-overlapping semantic atoms) and the most pronounced at stage 3 (18.3). This significantly impairs the interpretability of concepts and DVMs, and the explanations produced by concept-based XAI methods, underscoring the importance of quantifying concept polysemanticity and mitigating its impact on explanations.

As shown in Fig. S6 and exemplified in the first row of Table S8, compared with Fig. 3(a) in the main manuscript, there exist some concepts that require padding. Their commonalities display significant uniformity and an evenly distributed probability pattern, as discussed in Sec. S3.1. This phenomenon, where the actual level of polysemanticity is relatively low but is still calculated as high CPE,

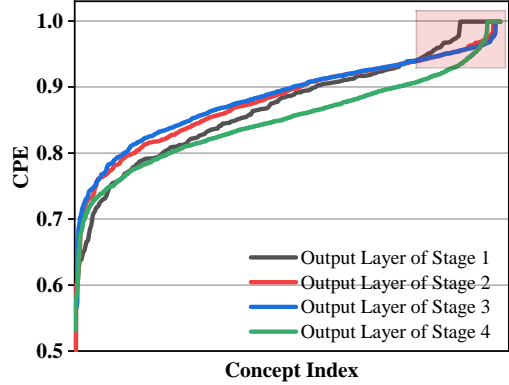


Figure S6. Clustered CPEs along the channel dimension. The channel indices are max-normalized. The magenta-highlighted regions emphasize results where commonalities are relatively limited, yet the computed CPE value is equal to 1.

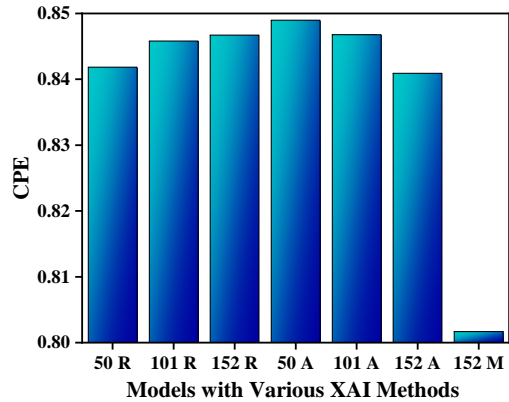


Figure S7. Averaged CPE scores on different XAI methods and different models. The number under the X-axis represents the model depth. R, A, and M stand for Relevance, Activation, and Maximum mutual information-based XAI Methods, respectively.

occurs more frequently in stages 1 and 4 of the DVM. As previously mentioned (discussed in Sec. 4.3 in the main manuscript), these stages are indeed characterized by generally lower levels of polysemanticity in their common concepts. After applying the padding operation, as illustrated in Fig. 3(a) in the main manuscript and the first row of Table S8, the corresponding CPE values drop to relatively low levels. This outcome further substantiates the effectiveness of the CPE proposed in this paper.

S4.2. Different XAI Methods

In this subsection, we conduct experiments on different XAI methods, including the relevance-based [2], activation-based [72], and maximal mutual information-based methods [34]. As illustrated in Fig. S7, the results reveal distinct trends in CPE across different XAI methods. Specifically, the polysemanticity observed in the activation-based

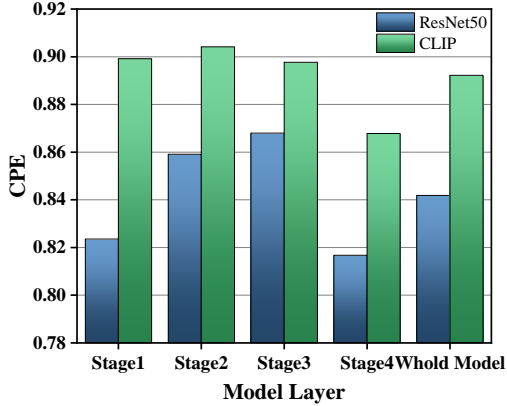


Figure S8. Averaged CPE scores on 2 model architectures, i.e., ResNet50 and CLIP.

method diminishes as model complexity increases, contrasting with the trend exhibited by the relevance-based method. This result indicates that the choice of the XAI method E_x is critical for concept-based explanations. Given that relevance-based concepts achieve superior fidelity and reliability in explanations compared to activation-based concepts [2], this paper adopts the relevance-based CRP as the primary E_x method. Moreover, concepts derived from maximal mutual information exhibit lower CPE values. However, due to the reliance on manually annotated concepts, this method lacks automation and flexibility, limiting its development on DVMs and hindering a more comprehensive comparison with other XAI methods. These results highlight the versatility of our approach in being applicable to various XAI methods and underscore the necessity of automating concept construction.

S4.3. Different Model Architectures

We calculate CPE values across different model architectures, including ResNet50 trained on ImageNet [19, 31] and CLIP-ResNet50 trained on a large-scale vision-language dataset [14, 51, 57]. As presented in Fig. S8, the vision branch of the CLIP model exhibits greater polysemanticity. The general trend aligns with that of the original ResNet, where polysemanticity is lowest in the abstract stage 4 and peaks in the intermediate stages. Polysemanticity is high in the shallowest stage. We infer that these results of CLIP-ResNet50 stem from the constructed global explanation dataset $ACD-B_{\mathcal{M},\mathcal{T}}$, which is derived from the Out-of-Distributed (OOD) ImageNet Validation dataset \mathcal{T} rather than the independent and identically distributed (iid) vision-language dataset utilized for CLIP’s training. Since CLIP operates in a zero-shot mode, the representation of each VC through 15 image patches does not fully align with the conceptual requirements of the original CLIP model, resulting in increased polysemanticity. Moreover, the vision-

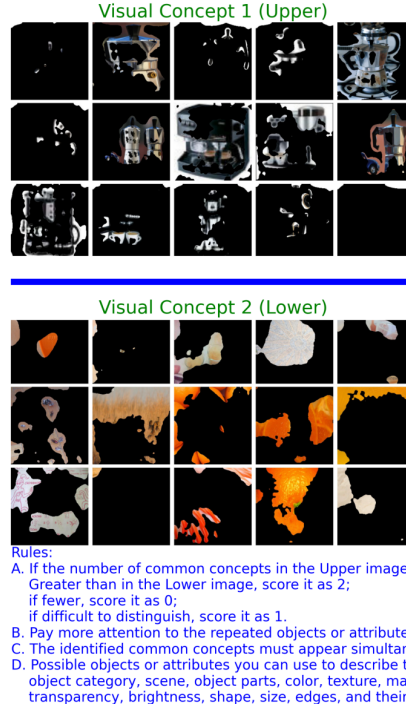


Figure S9. Examples of polysemanticity comparisons between human evaluations and CPE metric.

language dataset utilized for CLIP training encompasses significantly more categories and samples compared to the ImageNet dataset, resulting in an increase in the semantic scope that each concept must represent. This, in turn, amplifies the model’s polysemanticity. Our CPE method not only captures and precisely represents these phenomena through the lens of polysemanticity but also proves its effectiveness under zero-shot conditions, reinforcing the validity of the proposed approach.

S4.4. Human Evaluation on CPE

In this subsection, we present a comprehensive overview of the experiments conducted to perform human evaluations on the CPE metric. We first automatically generate a global concept explanation dataset $ACD-B_{\mathcal{M},\mathcal{T}}$ utilizing the CoE approach proposed in this paper. By incorporating the manually annotated MILAN ANNOTATION dataset [34], we construct a comprehensive VC library for this evaluation, comprising a total of 7,680 VCs. Recognizing the inherent difficulty for humans to directly quantify polysemanticity visually, we instead invite participants to compare the relative degrees of polysemanticity between two VCs. From this VC library, 300 pairs of VCs are randomly sampled, each displaying varying degrees of polysemanticity. As illustrated in Fig. S9, each pair is presented to human evaluators. Participants are instructed to assign a score of 2 if the upper VC exhibits more polysemanticity than the lower

Table S8. Additional examples of VCs and their disentangled concept atoms, along with their concept probability distributions and CPE scores. From top to bottom, the concepts displayed in the table are derived from concepts 141, 366, 1681, and 121 in the fourth stage of a ResNet152 model. The CPE values increase progressively from the top row to the bottom row.

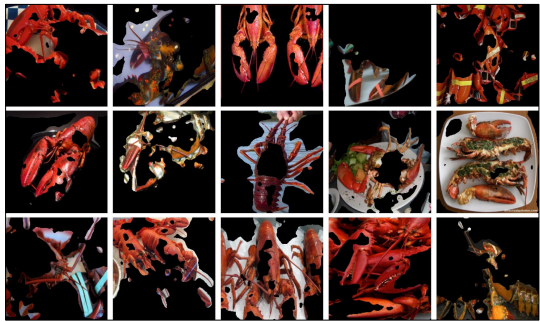
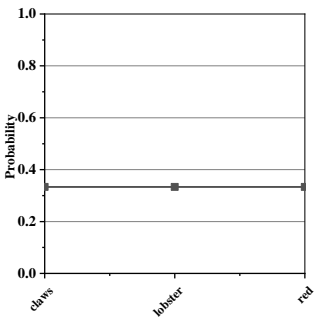
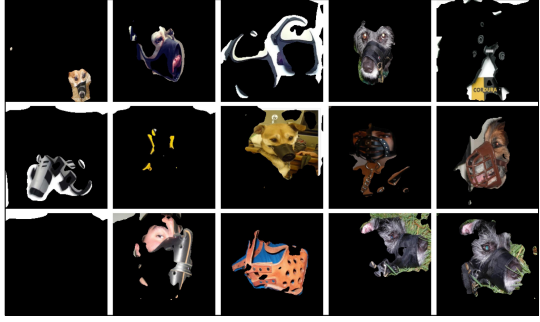
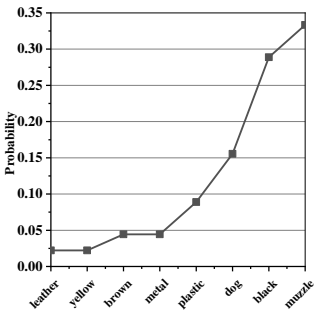
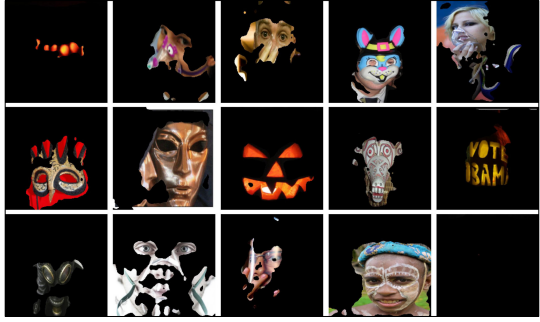
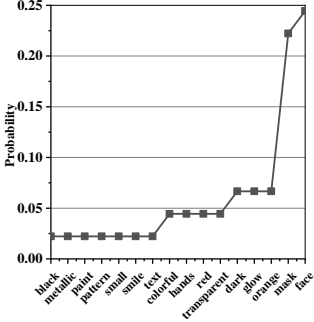
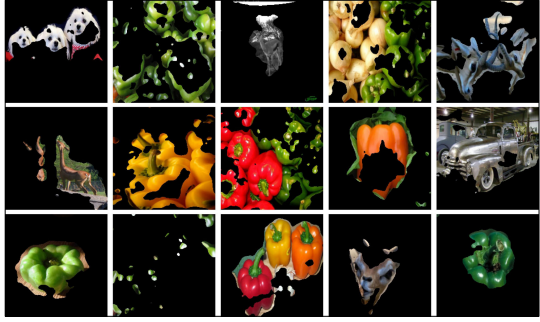
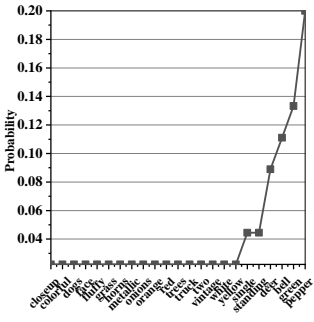
Visual Concept and Disentangled Concept Atoms				Concept Distribution	CPE
	Image 1: [lobster, red, claws], Image 2: [lobster, red, claws], Image 3: [lobster, red, claws], Image 4: [lobster, red, claws], Image 5: [lobster, red, claws], Image 6: [lobster, red, claws], Image 7: [lobster, red, claws], Image 8: [lobster, red, claws], Image 9: [lobster, red, claws], Image 10: [lobster, red, claws], Image 11: [lobster, red, claws], Image 12: [lobster, red, claws], Image 13: [lobster, red, claws], Image 14: [lobster, red, claws], Image 15: [lobster, red, claws]		0.70		
	Image 1: [dog, muzzle, black], Image 2: [dog, muzzle, black], Image 3: [muzzle, black, plastic], Image 4: [dog, muzzle, black], Image 5: [muzzle, black, plastic], Image 6: [muzzle, black, plastic], Image 7: [muzzle, black, yellow], Image 8: [dog, muzzle, black], Image 9: [muzzle, black, metal], Image 10: [dog, muzzle, brown], Image 11: [muzzle, black, plastic], Image 12: [muzzle, black, metal], Image 13: [muzzle, brown, leather], Image 14: [dog, muzzle, black], Image 15: [dog, muzzle, black]		0.77		
	Image 1: [orange, glow, dark], Image 2: [face, mask, colorful], Image 3: [face, mask, hands], Image 4: [face, mask, colorful], Image 5: [face, mask, transparent], Image 6: [mask, red, black], Image 7: [mask, metallic, face], Image 8: [orange, glow, face], Image 9: [mask, face, pattern], Image 10: [orange, glow, text], Image 11: [mask, goggles, dark], Image 12: [face, mask, transparent], Image 13: [face, mask, hands], Image 14: [face, paint, smile], Image 15: [dark, small, red]		0.85		
	Image 1: [white, fluffy, dogs], Image 2: [green, bell, peppers], Image 3: [deer, standing, trees], Image 4: [onions, green, peppers], Image 5: [two, deer, horns], Image 6: [deer, standing, grass], Image 7: [yellow, bell, peppers], Image 8: [red, green, peppers], Image 9: [orange, bell, peppers], Image 10: [metallic, vintage, truck], Image 11: [single, green, pepper], Image 12: [green, bell, peppers], Image 13: [colorful, bell, peppers], Image 14: [deer, face, closeup], Image 15: [single, green, pepper]		0.88		

Table S9. Explainability metrics utilized for evaluating the local explanations. These criteria are prompted for both GPT-4o and human-based scoring systems. Each criterion has a maximum score of 2 points. The total explanation score is 6. The **bolded** areas represent the core decision rationale for the scoring process.

Metrics	Score	Details of Each Criterion
Accuracy	2	Almost all relevant explanations focused on key decision points, essential features, important regions, and background information, with no extraneous or irrelevant content.
	1	Explanation is generally relevant but may contain some minor off-topic or unnecessary information.
	0	Explanation includes a significant amount of irrelevant content, diverging from the model’s decision-making process and impairing comprehension.
Completeness	2	Comprehensive explanation covering all major steps , key features, background information, and relevant concepts of the model’s decision process.
	1	Explanation addresses primary decision steps but may slightly overlook some information or secondary features.
	0	Incomplete explanation lacking essential decision steps or information, making comprehension challenging.
User Interpretability	2	Explanation allows users without specialized knowledge to understand the model’s decision logic, with clear, straightforward language and smooth readability.
	1	Explanation is mostly understandable to users with a technical background ; it is fairly clear but may require some re-reading due to less fluent phrasing or logic.
	0	Explanation is difficult to comprehend , with disorganized or unclear language that obscures the decision process of the model.

one, a score of 1 if the opposite is true, and 1 if the distinction is unclear. The evaluation guidelines also prompt 13 feasible semantic directions and rules consistent with those prompted for the CPE metric. All VC pairs are divided into 10 groups, with each group evaluated by three participants. If the average score exceeds 1, the upper VC is judged to have greater polysemanticity than the lower one; otherwise, it is assigned a score of 0. Consistency between these results and the CPE metric is then calculated, as summarized in Table 2 in the main manuscript. The results reveal a 75% agreement between human evaluations and the CPE metric, thereby demonstrating the validity of the CPE method.

S4.5. Examples of Disentanglement and CPE

In this subsection, we present additional examples illustrating the disentanglement of VCs into concept atoms, as well as the probability distributions and CPE values of the clustered atoms. As shown in Table S8, the experimental results align with the analyses presented in Sec. 4.2 in the main manuscript. The proposed CoE approach effectively and accurately disentangles VCs into linguistic concept atoms. Furthermore, the entailment model successfully clusters semantically equivalent atoms into mutually

orthogonal groups, assigning corresponding probabilities to them. The proposed CPE metric quantifies the polysemanticity of different VCs, with the subjective visual comparisons and the CPE results demonstrating consistent trends. The polysemanticity of the VCs in the table increases progressively from the first row to the last. Correspondingly, the disentangled atoms, their associated probabilities, and the CPE values exhibit consistent changes in alignment with this trend. These results collectively validate the effectiveness of the approach proposed in this paper.

S5. Experiments on CoE Local Explanations

In this section, we elaborate on the evaluation employed to assess the linguistic local explanations. We also present and compare additional instances of local explanations generated by CoE and other methods.

S5.1. Evaluation of Local Explanations

The local explanations are evaluated from three explainability evaluation metrics, namely, Accuracy, Completeness, and User Interpretability [61]. We exclude the fidelity criterion, as CoE finds the key concepts of DVMs through existing concept circuit methods, inherently aligning its fidelity

Table S10. Comparisons of GPT-4o explanation scores under various scenarios. †: the results of baselines are obtained by applying ACD and local explanation steps, without CPDF.

Method	Accuracy	Completeness	User Interpretability	Total Explanation
Places365 Dataset [73] (Baseline†)	1.01	1.07	1.04	3.12
CoE on Places365 Dataset (Ours)	1.68	1.69	1.67	5.04
Chest X-ray Dataset [65] (Baseline†)	1.55	1.62	1.56	4.73
CoE on Chest X-ray Dataset (Ours)	1.81	1.74	1.76	5.31
ViT-B-16 [4] (Baseline†)	1.18	1.14	1.16	3.48
CoE on ViT-B-16 (Ours)	1.65	1.69	1.58	4.92

Table S11. GPT-4o scores on other concept explanation methods.

Method	Acc.	Comp.	User I.	Total
CLIP-Dissect[48] +Descrip.	1.10	1.13	1.08	3.31


with these approaches. Each metric is assigned three score levels: 2 points for optimal performance, 0 points for the lowest performance, and 1 point for a moderate score, as presented in Table S9. The maximum score for each metric is 2, with a total possible score of 6.

These evaluation criteria are provided to both human evaluators and GPT-4o to score the generated linguistic local explanations. To construct the database for GPT-4o-based evaluation, 500 samples are randomly selected from the ImageNet Validation dataset. We sample from the correctly and incorrectly predicted instances of the DVM in a 7:3 ratio, in alignment with the accuracy rate. Three methods, including baseline, CoE without filtering, and CoE, are evaluated in this paper. They generate local explanations for these samples. The evaluation prompt for GPT-4o is discussed in Sec. S2.3. Given the complexity of this evaluation for humans, we randomly select 100 samples from the former database to construct the database for human-based evaluation. The evaluation page, as shown in Fig. S10, consists of the sampled image, the generated local explanations, and the scoring criteria for the three explainability metrics. The three methods are anonymously labeled as Ex1, Ex2, and Ex3. As for human evaluations, the 100 samples are divided into 10 groups, with each group consisting of 30 linguistic explanations assessed by three participants. The results, presented in Table 4 in the main manuscript, demonstrate that the CoE approach outperforms the other two methods across all three explainability metrics, confirming the superiority of the proposed approach.

S5.2. Supplemental Quantitative Evaluation Results

We conduct experiments of CoE on a Transformer architecture (i.e., ViT-B-16) [4]. As shown in the 6th row of Table S10, CoE is effective for the Transformer architecture, achieving an improvement of 1.44 points compared to its

CoE Local Explanation Group A-2 img10168 Ex1



The model outputs a correct result: West Highland white terrier. Specifically, in the shallowest layer 1 of the model, channel 88 with a relevance value of 1.0 describes the concept of 'curved', which might be related to the curved features of the dog's body or face. In the deeper layer 2 of the model, channel 103 with a relevance value of 1.0 describes the concept of 'face', channel 94 with a relevance value of 0.74 describes the concept of 'background', and channel 162 with a relevance value of 0.73 describes the concept of 'animal'. These concepts are essential for identifying the presence and type of animal in the image. In layer 3, channel 985 with a relevance value of 1.0 describes the concept of 'texture', channel 174 with a relevance value of 0.85 describes the concept of 'white', and channel 880 with a relevance value of 0.77 describes the concept of 'fur', which are all highly relevant to the appearance of a West Highland white terrier as described in the image caption. Finally, in layer 4, channel 1230 with a relevance value of 1.0 describes the concept of 'dog', and channel 1280 with a relevance value of 0.87 describes the concept of 'sitting', aligning perfectly with the caption description of the dog's posture and identity. Therefore, the model outputs a correct result West Highland white terrier, as all these concepts are related to the dog breed in the image.

Criteria	Your Score
1. Explanation Accuracy [2,1 or 0]:	
2. Explanation Completeness [2,1 or 0]:	
3. User Interpretability [2,1 or 0]:	
Total Score [0-6]	

Figure S10. Examples used for evaluating the local explanations generated by three methods.

baseline (the 5th row). Besides, CoE is tested on two other real-world and critical applications (i.e., Places365 [73] and Chest X-ray [65]). Table S10 demonstrates CoE's consistent superiority, achieving scores of 5.04 and 5.31 with improvements of 1.92 and 0.58 over their baselines (without considering polysemanticity). In the medical dataset Chest X-ray [65], CoE achieves an explanation score of 5.31 since the category variety in this dataset is relatively small. All the images depict the human thoracic cavity, and the differences between categories are minimal. This implies that the polysemanticity of concepts learned within the network is more advantageous, enhancing the explainability. We also compare a CLIP-Dissect [48] method for describing concepts, published in ICLR 2023. As shown in Table S11, the overall explainability score is 3.31, which is clearly lower than that of CoE (5.06). CLIP-Dissect generates a single concept atom per channel, which severely underestimates the polysemanticity issue, resulting in insufficient explanations. All results demonstrate the robustness and scalability of the proposed CoE approach.

S5.3. Examples of CoE Local Explanations

In this subsection, we present additional samples to demonstrate the effectiveness of the proposed CoE approach in explaining the decision-making process of DVMs. As presented in Table S12, the experimental results align with the

analyses in Sec. 4.4 in the main manuscript. Nearly all concepts are closely associated with the input images. It infers the logical relationship between the current concept and the entire context according to its contents and relevance values. The final output explanations accurately articulate the decision pathways underlying the DVM’s predictions.

S5.4. Comparison Between CoE and Baseline

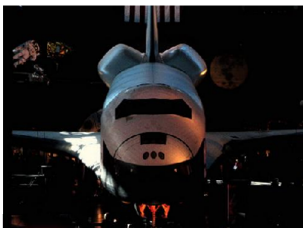
Additionally, we provide a comparative analysis of CoE-based local explanations with that generated by the baseline method. As exemplified in Table S13, the concepts provided from the baseline method exhibit inconsistencies with the input images, highlighting that disregarding polyseman- ticity undermines the comprehensibility of local explanations. In contrast, the CoE approach generates linguistic explanations that encapsulate all indispensable relevant in- formation for identifying a hog, such as the concept of pig and pink. These results collectively validate the effective- ness and superiority of the CoE approach proposed in this paper.

Table S12. Additional cases of local explanations generated from the CoE approach. The first three rows show the explanations of correct predictions of the DVM, and the fourth row is reversed. The yellow highlighted regions illustrate the logical relationships identified by the CoE approach between concepts within the explanation chains and between concepts and their contexts. The green highlighted regions represent the CoE approach’s final summary and commentary on the explanation chains.



label: stone wall
 predict: stone wall

The model outputs a correct result: stone wall. Specifically, in the shallowest layer 1 of the model, channel 88 with a relevance value of 1.0 describes the concept of smooth, and channel 3 with a relevance value of 0.83 describes the concept of ground. **These initial detections are fundamental as they set the stage for recognizing more complex features.** In the deeper layer 2 of the model, channels such as 401 with a relevance value of 1.0 and 103 with a relevance value of 0.95 both describe the concept of edges, **which are crucial for identifying the boundaries and shapes within the stone wall.** Channels 24 and 391 with relevance values of 0.91 and 0.84 respectively describe rocks, and channel 26 with a relevance value of 0.73 describes stone, **further honing in on the key components of the wall.** Channel 506 with a relevance value of 0.72 describes the wall, **integrating these features into the overall structure identified in the image.** In layer 3, channel 985 with a relevance value of 0.87 describes texture, **which is important for recognizing the surface characteristics of the stone wall.** Finally, in layer 4, channels 1723 and 1260 with relevance values of 1.0 and 0.81 respectively both describe the wall and stone, **confirming the identification of the image as a stone wall.**
 The model's decision path aligns well with the ground truth and the detailed description provided in the caption, leading to a correct prediction.



label: space shuttle
 predict: space shuttle

The model outputs a correct result: space shuttle. Specifically, in the shallowest layer 1 of the model, channel 88 with a relevance value of 1.0 describes the concept of 'smooth', **which aligns with the smooth surfaces typically seen on space shuttles.** In layer 2, channel 103 with a relevance value of 1.0 describes the concept of 'stars', **which could relate to the space context of the shuttle,** and channel 166 with a relevance value of 0.74 describes 'wooden', **which might be less relevant here but could be linked to the indoor display setting of the shuttle.** In layer 3, channels 985 and 911 with relevance values of 1.0 and 0.76 respectively describe 'display' and 'background', **correctly identifying the shuttle's display context and its background setting in the image.** Channels 525 and 233, both describing 'metal' and 'metallic' with relevance values of 0.71 and 0.7, **align well with the typical materials used in the construction of a space shuttle.** Finally, in the deepest layer 4, channel 1494 with a relevance value of 1.0 accurately identifies the object as a 'shuttle', and channel 625 with a relevance value of 0.85 describes the color **'white', matching the primary color of the shuttle in the image.**
 The model's decision path and the high relevance values of the key concepts directly related to the features of a space shuttle, such as its material and context of display, support the correctness of the prediction. Therefore, the model outputs a correct result: space shuttle.



label: steel arch bridge
 predict: steel arch bridge



The model outputs a correct result: steel arch bridge. Specifically, in the shallowest layer 1 of the model, channel 88 with a relevance value of 1.0 describes the concept of orange, **which corresponds to the orange sky described in the image caption.** In the deeper layer 2 of the model, channel 401 with a relevance value of 1.0 describes the concept of curved, channel 404 with a relevance value of 0.75 describes the concept of sunset, channel 182 with a relevance value of 0.72 describes the concept of water, and channel 103 with a relevance value of 0.71 describes the concept of yellow. **These concepts align well with the image description, capturing the curved shape of the bridge, the sunset, and the water reflection.** In layer 3, channel 395 with a relevance value of 1.0 describes the concept of cloud, and channel 725 with a relevance value of 0.76 further supports the concept of sunset, **enhancing the contextual understanding of the scene.** Finally, in layer 4, channels 1120 and 573 both with high relevance values (1.0 and 0.92 respectively) describe the concept of **bridge, directly identifying the main object in the image.**
 The structured and high relevance of these concepts at each layer demonstrates a clear and accurate recognition path from general scene attributes to the specific identification of the steel arch bridge, confirming the correctness of the model's prediction.



label: gar
 predict: pencil box

The model outputs an incorrect result pencil box instead of the correct label gar. Specifically, in the shallowest layer 1 of the model, channel 88 with a relevance value of 1.0 describes the concept of orange, **which may relate to the orange lines mentioned in the image caption.** In the deeper layer 2, channel 229 with a relevance value of 1.0 correctly identifies the concept of fish, **aligning with the caption that describes a large fish.** Moving to layer 3, channels 422 and 31 with relevance values of 1.0 and 0.99 respectively **continue to support the identification of the object as a fish and an animal.** However, channel 519 with a relevance value of 0.82 describes the concept of measurement, **likely influenced by the presence of a ruler in the image, which is a common object in a pencil box.** In layer 4, channel 1147 with a relevance value of 1.0 describes the concept of black, **possibly picking up on the black cap mentioned in the caption,** and channel 626 with a relevance value of 0.74 **describes the concept of ruler.**
 The model seems to have been misled by the presence of objects typically found in a pencil box (ruler, black cap) and the concept of measurement, leading it to incorrectly predict the image as a pencil box rather than recognizing the primary subject as a gar fish. Therefore, the model outputs an incorrect result pencil box.

Table S13. Comparisons between local explanations generated by the baseline method and our CoE approach. The highlighted regions indicate the key concepts identified by different methods as influential in the model’s decision-making process. The local explanations in the first row are generated by the baseline method using the manually annotated MILAN ANNOTATION dataset, while the second row represents the outputs of our CoE approach applied to the automatically constructed ACD- $\mathcal{B}_{M,T}$ dataset.

<p>MILAN ANNO. (Baseline)</p>		<p>The model outputs a correct result hog. Specifically, in the shallowest layer 1 of the model, channel 88 with a relevance value of 1.0 describes the concept of a bear running across sand and a dog going through the pasture with flowers, which might not directly relate to the image of piglets but could be triggered due to the presence of animals in motion or in a pastoral setting. In the deeper layer 2 of the model, channel 46 with a relevance value of 0.82 describes the concept of animals, which directly correlates to the image content of piglets. Furthermore, in layer 4 of the model, channel 475 with a relevance value of 0.75 describes the concept of pictures of animals, which strongly supports the correct identification of the image as containing animals, specifically hog. The decision path and relevance values indicate that the model has effectively recognized the primary subject (animals) in the image, leading to the correct prediction of hog, aligning with the ground truth label and the image caption describing piglets.</p>
<p>CoE (Ours)</p>		<p>The model outputs a correct result: hog. Specifically, in the shallowest layer 1 of the model, channel 88 with a relevance value of 1.0 describes the concept of 'smooth', which may relate to the texture of the piglets in the image. In the deeper layer 2 of the model, channels 391, 506, 46, 26, and 24 with relevance values of 1.0, 0.88, 0.82, 0.77, and 0.75 respectively, all describe the concept of 'animal', aligning well with the presence of piglets in the image. Channel 229 with a relevance value of 0.77 describes the concept of 'grid', which corresponds to the wire fence enclosure mentioned in the caption. Channel 402 with a relevance value of 0.71 describes 'food', which is consistent with the description of one piglet eating. In layer 3, channel 985 with a relevance value of 1.0 continues to describe 'grid', reinforcing the identification of the enclosure. Channels 591 and 498 with relevance values of 0.96 and 0.78 describe 'creature' and 'animal' respectively, further confirming the presence of living animals in the image. Finally, in layer 4, channels 726 and 475 with relevance values of 1.0 and 0.75 describe 'pig', and channel 1884 with a relevance value of 0.84 describes 'pink', directly correlating with the pink piglets observed. These concepts are all highly relevant to the image's content as described in the caption, leading to a correct prediction of 'hog'.</p>